

Detailed Far-UV to Optical Analysis of Four [WR] Stars

W. L. F. Marcolino¹

wagner@on.br

D. J. Hillier²

hillier@pitt.edu

F. X. de Araujo¹

araujo@on.br

and

C. B. Pereira¹

claudio@on.br

ABSTRACT

We present far-UV to optical analyses of four hydrogen deficient central stars of planetary nebulae : BD +30 3639, NGC 40, NGC 5315 and NGC 6905. Using the radiative transfer code CMFGEN, we determined new physical parameters and chemical abundances for these stars. The results were analyzed in the context of the [WR] \rightarrow PG 1159 evolution via the transformed radius-temperature ($R_T \times T_*$) and HR diagrams. We found that the use of clumping increases R_T by up to ~ 0.5 dex relative to previous results, whilst our homogeneous models showed systematic changes of $\sim 0.1 - 0.2$ dex. NGC 5315 showed itself as an odd object among the previously analyzed central stars. Its temperature ($\sim 76kK$) is considerably lower than other early-type [WR] stars ($\sim 120 - 150kK$). From our

¹Observatório Nacional, Rua Gen. José Cristino 77, 20921-400, Rio de Janeiro, Brazil

²Department of Physics and Astronomy, University of Pittsburgh, Pittsburgh, PA 15260

models for NGC 5315 and NGC 6905, it is unclear if early-type [WR] stars have smaller C/He mass ratios than other spectral classes, as claimed in the literature. In particular, the ratio found for NGC 6905 (~ 0.8) is in rough agreement with evolutionary calculations, and with values derived for [WCL] stars. We analyzed FUSE spectra of these stars for the first time, and identified phosphorus in the spectra of BD +30 3639, NGC 40 and NGC 5315 through the doublet transition P V $\lambda\lambda 1118, 1128$ ($3p \ ^2P^o - 3s \ ^2S$). The iron, silicon, phosphorus, sulfur and neon abundances were analyzed in the context of the nucleosynthesis occurring in previous evolutionary phases. We found evidence for an iron deficiency in BD +30 3639 and NGC 5315, and from fits to the Si IV lines we determined a solar silicon abundance for BD +30 3639 and NGC 40. For phosphorus, an oversolar abundance in the NGC 5315 model was preferred, while in the other stars a solar phosphorus abundance cannot be discarded. Regarding sulfur, we estimated upper limits for its abundance, since no conspicuous lines can be seen in the observed spectra. We found that neon is overabundant in BD +30 3639. In the other stars, neon is weak or undetectable and upper limits for its abundance were estimated. Our results are in agreement with theoretical predictions and show the usefulness of [WR] stars as testbeds for nucleosynthesis calculations in the AGB and post-AGB phases.

Subject headings: stars:fundamental parameters - stars:post-AGB - stars:Wolf-Rayet - planetary nebulae:general

1. Introduction

Hydrogen deficient central stars of planetary nebulae (CSPN) present a challenge to stellar evolution theory: it is still unclear how a star removes its hydrogen when going from the AGB to the planetary nebula stage. One of the first theories trying to explain this phenomenon was proposed by Iben et al. (1983). In their *born-again* scenario, a very late thermal pulse (VLTP) occurs in the white dwarf cooling track of the HR diagram. As a consequence, all the remaining hydrogen is burned and the star is driven to red giant dimensions, near the AGB, for a second time. Two other thermal pulses could also potentially give rise to hydrogen deficient CSPN. One is the AFTP (AGB final thermal pulse), occurring at the end of the AGB phase, and the other is the LTP (late thermal pulse), which occurs when the star is already on the post-AGB track. It seems that all three scenarios are necessary in order to explain the wide range of hydrogen deficient CSPN properties (e.g., hydrogen abundance and nebular diameters), and that there is no unique mechanism or

single channel of evolution (Blöcker 2001; Herwig 2001).

Binarity could also provide an avenue for the creation of hydrogen deficient CSPN. De Marco & Soker (2002), for example, raised the interesting possibility of a companion engulfed by an AGB star. In this way, extra mixing would be induced and a hydrogen deficiency would be achieved. However, the scenario is still speculative and lacks quantitative calculations.

The evolutionary sequence of hydrogen deficient CSPN is also uncertain. Generally these objects are divided into three classes : [WR], [WC]-PG 1159 and PG 1159 stars. [WR] stars show spectra very similar to Wolf-Rayet stars of Pop. I, with strong and broad emission lines. [WC]-PG 1159 stars show both absorption and weak emission lines in their optical spectra, while wind features are seen in the UV. Parthasarathy et al. (1998) claim that [WC]-PG 1159 and the *weak emission line stars* ([WELS]), presented in the work of Tylenda et al. (1993), constitute the same class. PG 1159 stars show mainly absorption lines in their spectra.

Analysis of the spectra of the central stars or of their nebulae seems to indicate the following evolution : [WCL] \rightarrow [WCE] \rightarrow [WC]-PG 1159 = [WELS] \rightarrow PG 1159 (Werner & Heber 1991a,b; Zijlstra et al. 1994; Gorny & Tylenda 2000; Peña et al. 2001; Leuenhagen et al. 1996; Koesterke & Hamann 1997a,b; Leuenhagen & Hamann 1998). However, there are still fundamental questions to be addressed. A major problem is the C/He mass ratio obtained for early-type [WR] stars, which is ~ 0.35 on average. This is lower than found in the other classes, and is thus in contradiction to the above evolutionary sequence. It also disagrees with evolutionary models which find this ratio to be ~ 1 (Herwig 2001). A second problem comes from the work of Gorny & Tylenda (2000), who showed that some stars might not follow this evolution channel. Through an analysis of nebular parameters, the authors suggest that some objects that have experienced the VLTP could evolve directly to the PG 1159 stage without becoming [WC] stars. Another important problem is that the role of the [WELS] is not yet understood (Marcolino & de Araújo 2003). Indeed, Peña et al. (2003a,b) were able to show that nebular expansion velocities of [WC] stars are generally higher than for the [WELS], in contradiction to that expected from [WC] \rightarrow [WELS] evolution. Moreover, the presence of hydrogen is still questionable (De Marco & Barlow 2001) and can favor a specific thermal pulse model. While in the AFTP and LTP a small amount is found, in VLTP models the hydrogen is completely burnt.

So far, the majority of [WR] stars analyzed by means of non LTE expanding atmosphere models is due to the Potsdam group code (see Koesterke 2001 and references therein). Additional studies of three [WCL] stars were undertaken by De Marco & Crowther (1998, 1999) using an independent code (CMFGEN, Hillier & Miller 1998). All objects were studied without metal line-blanketing or clumping (exceptions are the recent work of Stasińska et al.

2004 and of Peña et al. 2004 regarding two stars on LMC, Herald & Bianchi 2004a,b, which included one [WC4] and two [WC]-PG 1159 stars and Crowther et al. 2006, who compared the [WC9] star BD +30 3639 with the Wolf-Rayet star HD 164270). These two effects have been shown to be very important when analyzing hot stars with winds (Hillier & Miller 1998, 1999; Gräfener et al. 2002), having an impact on important physical parameters (e.g., T_{eff} and \dot{M}).

With the aim of addressing some of the problems and uncertainties discussed above, we have derived physical parameters and chemical abundances of a small sample of H deficient CSPN (BD +30 3639, NGC 40, NGC 5315 and NGC 6905) using the CMFGEN code developed by Hillier & Miller (1998). Contrary to most of the previous works on CSPN, line-blanketing and clumping are taken into account in the models. We also rely on improved atomic data and fits to larger spectral intervals, including the FUSE region now available for some CSPN. Among the issues that we address are : the influence of line-blanketing and clumping on the evolutionary sequence; the peculiar values of the C/He mass ratio for the early-type [WR] stars and the iron abundance and its possible depletion as predicted by AGB and post-AGB evolutionary calculations.

This paper is organized as follows. The observational data is described in Section 2. In Section 3 we explain the code used (CMFGEN) and its main assumptions, while in Section 4 we present our analysis from the far-UV to the optical for each object. In Section 5 we discuss our results. Finally, in Section 6 we summarize the main points of our work.

2. Observations

The optical data of BD +30 3639 and NGC 5315 were obtained in 2000 using the Boller & Chivens spectrograph at the Cassegrain focus on the 1.52m ESO telescope in La Silla, Chile. The resolution is about 2\AA in the spectral range $\sim 4000 - 6000\text{\AA}$. The spectra were reduced using IRAF. Default procedures such as bias and sky subtraction, spectral extraction and flat-field corrections were taken into account. He, Ar and Fe lamps were used to provide wavelength calibration for every stellar frame. More details can be found in our previous paper (de Araújo et al. 2002). The spectra of NGC 40 and NGC 6905 were kindly provided by Paul A. Crowther. They were observed on the 2.5m Isaac Newton Telescope (INT) in La Palma, Spain. The spectral interval is $\sim 3600 - 6800\text{\AA}$ and the resolution is $\sim 1.5\text{\AA}$ for NGC 40 and $\sim 3\text{\AA}$ for NGC 6905. Further details can be found in Crowther et al. (1998).

In the ultraviolet and far-ultraviolet region, we used public data from the Multi-mission

Archive at STScI (MAST) ¹ from the IUE and FUSE satellites. The wavelength coverage is 1087 – 1182Å (also 980 – 1182Å in NGC 6905) for FUSE spectra and \sim 1100 – 3200Å for IUE spectra. All FUSE spectra were co-added and smoothed with a 3-5 point average for a better signal-noise ratio and clarity, respectively. The resolution of the models shown in the next sections was chosen to match the resolution in each observed spectrum.

3. Model atmosphere

The physics present in hydrogen deficient CSPN is very complex. CSPN have high effective temperatures (\sim 20 – 200kK), intense radiation fields and expanding atmospheres. These necessitate, at a minimum, the use of spherical expanding non LTE model atmospheres. Moreover, the presence of clumps (enhanced density regions, i.e., *clumping*) is predicted by radiation hydrodynamic theory (Owocki 1994) and supported by observational studies (see for example Bouret et al. 2005 and references therein) which invalidates the commonly adopted hypothesis of a smooth outflow.

For our analyses we used the non LTE radiative transfer code, CMFGEN (Hillier & Miller 1998). CMFGEN solves the radiative transfer equation, in a spherically symmetric expanding outflow, simultaneously with the statistical and radiative equilibrium equations. It has been applied to the study of several classes of objects where non LTE conditions and a stellar wind are present (e.g., WR, LBV and O stars). More recently, CMFGEN was used to investigate the photospheric phase of type II supernovae (Dessart & Hillier 2005).

Line-blanketing is known to change the atmospheric structure of WC stars and it affects important lines such as C III λ 5696 and C IV $\lambda\lambda$ 5801, 5811, which are used in classification schemes (Crowther et al. 1998; Acker & Neiner 2003). To facilitate the inclusion of metal line-blanketing in CMFGEN, *super-levels* are used. In this formalism, levels with similar properties are treated as one and have the same departure coefficient, saving a considerable amount of computer memory and time. In the atomic model for Fe IV, for example, 1000 levels could be reduced to 100. Models with different super-levels assignments were tested in order to check for differences in the theoretical spectra.

Clumping is incorporated into CMFGEN using a volume filling factor (f) approach (Hillier & Miller 1999). In all models of this work we assume $f = 0.1$. Evidence for clumping in spectral fits can be primarily seen in the red wings of emission lines, although a few individual line strengths and profiles can also show some sensitivity. Clumping tends to

¹<http://archive.stsci.edu/>

reduce the derived mass-loss rates by a factor of $\sim 3 - 5$. While a non-clumped wind can be ruled out by the modeling, it is difficult to derive an accurate clumping value. Consequently, we always tabulate both the derived mass-loss rate and the unclumped value \dot{M}_{uncl} ($=\dot{M}/\sqrt{f}$). Models with fixed \dot{M}_{uncl} generally show very similar spectra. In some objects of our sample (BD +30 3639 and NGC 40), direct evidence for clumping has been obtained from observations of moving features on the top of some specific lines (see for example, Grosdidier et al. 2000).

In order to improve the modeling of C II lines we implemented new autoionization data made available by the Auburn-Rollins-Strathclyde collaboration², which is not included in Opacity Project Calculations.

4. Analysis

The main input parameters in a CMFGEN model are the luminosity (L), the radius (R_*), the mass-loss (\dot{M}), the velocity law [$v(r)$] and the chemical abundance. The stellar temperature T_* follows from the relation $L = 4\pi R_*^2 \sigma T_*^4$ and the effective temperature T_{eff} is defined where the Rosseland optical depth is $2/3$. In order to explore these parameters in an efficient way, we adopted the following strategy for our analyses. As the distances involved are not precisely known, we chose to fix the luminosity in $5000L_\odot$ in our models. This particular choice of L was made as it is the approximate value found from the evolution of a main sequence star of $\sim 3M_\odot$ (Blöcker 2001; Althaus et al. 2005). With the luminosity fixed, the distance was derived from the continuum spectral fit. If a reliable distance is determined for one of the stars of our sample, the physical parameters derived by our analysis can be scaled to new values by keeping the so-called *transformed radius* and T_{eff} constant (Schmutz et al. 1989; Hillier & Miller 1999; see §5.3). We then investigated different stellar temperatures by changing the radius of the star. The velocity law used was a simple β -law ($\beta = 1$) and v_∞ was fixed by the blue shifted absorption in a P-Cygni profile or by values found in the literature. Thereafter, we changed the mass-loss until we obtained a satisfactory fit. Abundance changes were the last step on the modeling process. The C/He ratio was derived mainly from the fit to the He II $\lambda 5412$ and C IV $\lambda 5471$ transitions. In some cases we found that the best fit to these lines yielded a poor fit to other lines (e.g. C III $\lambda 5696$). In such cases we chose to determine the abundance by the overall spectral fit. Because a perfect match to the observed spectra is not possible, a quality judgment was exercised to choose our final models.

²Auburn-Rollins-Strathclyde Dielectronic Recombination Data - <http://www-cfadc.phy.ornl.gov/>

We generally started with simple atomic models (e.g., He, C, O and Fe ions) and we gradually added and tested the influence of new elements on the spectrum. This approach helped to determine and fit previously unidentified features, such as P V and Al III in the ultraviolet. We did not include hydrogen in our analysis. Its presence in [WR] stars is very difficult to determine and it is still a matter of debate. The ions considered in the final model for BD +30 3639 are shown in Table 1 as an example. We included a total of 4428 full-levels, which were reduced to 1391 with the use of super-levels. For the other stars, only a few modifications were done to the atomic model. We now discuss the analysis of the individual stars: BD +30 3639 (§4.1), NGC 40 (§4.2), NGC 5315 (§4.3) and NGC 6905 (§4.4).

4.1. BD +30 3639

BD +30 3639 (also called Campbell’s star) is a well studied planetary nebula that has a [WC9] central star. It is one of the few planetary nebulae with detected X-ray emission (Arnaud et al. 1996; Kastner et al. 2000; Maness et al. 2003), and, unusually, it has both oxygen and carbon-rich dust envelopes (Waters et al. 1998). Further, it has high velocity molecular knots: the first detected in a planetary nebula (Bachiller et al. 2000). Despite efforts to understand its nature and evolution only a few studies have focused on its central star.

Leuenhagen et al. (1996) were the first to use non LTE expanding atmosphere models to obtain, based primarily on optical line fits, physical parameters and chemical abundances for BD +30 3639. Their model atmosphere considered only H, He, C and O ions, and at that time, they were unable to include line-blanketing and clumping. The presence of clumping in BD +30 3639 was reported by Acker et al. (1997) and Grosdidier et al. (2000) through the study of moving features on the top of the C III λ 5696 line.

Recently, Crowther et al. (2006) also analyzed this star using CMFGEN. However the study primarily focused on the Population I Wolf-Rayet star HD 164270, and a comparison was made with BD +30 3639 because of their identical spectral classification (WC9). Here emphasis is given to the determination of physical parameters, chemical abundances and the star’s evolutionary state.

4.1.1. *Optical and ultraviolet fit*

In Fig. 1 we show the observed and theoretical optical spectra. The distance derived from our fit is 1.2kpc, which is the same value found by Li et al. (2002) using Hubble

Space Telescope observations of the expansion of the nebula of BD +30 3639. In the 4000 – 5000Å range we have a reasonable agreement between model and observations, but we had difficulties in fitting the observed 4650Å profile simultaneously with the other features. This blend is formed by C III and C IV transitions and it is weaker in the model than in the observed spectrum. On the other side, our model provides a very good fit to the 5000–6000Å interval. The C III λ 5696 line was only reproduced after the inclusion of clumping (with $f = 0.1$). The He I λ 5876 profile is contaminated by the nebula. In this case, a resolution higher than 2Å would be necessary in order to better separate wind and nebular emissions.

The far-ultraviolet spectrum from FUSE and our model are shown in Fig. 2 (top). We used only the LiF2A channel ($\sim 1087 - 1182\text{\AA}$) which is free of severe interstellar contamination. This is the first spectral analysis of this object in this region. Our main findings are the P-Cygni profiles in λ 1118 and λ 1128, which were only fitted after the inclusion of phosphorus (P V). The determination of the phosphorus abundance is important in the context of nucleosynthesis during the AGB evolution and will be discussed later in the paper. Our models also indicate a silicon contribution in 1128Å from Si IV.

The high-resolution spectrum from the IUE satellite is also shown in Fig. 2 along with our model. The observed continuum near 1200Å does not match between IUE and FUSE spectra. The FUSE continuum is higher $\sim 5 \times 10^{-13} \text{ ergs cm}^{-2} \text{ s}^{-1} \text{ \AA}^{-1}$. We could only achieve agreement between observed and theoretical spectrum from the far-UV to the optical using slightly different values for E(B-V) ($\sim 0.34 - 0.40$). Errors in flux calibrations and uncertainties in the extinction law are probably reasons for the discrepancy. It is known, for example, that BD +30 3639 has a dusty halo which contributes to its own extinction (Harrington et al. 1997).

The most prominent features in the $\sim 1100 - 2000\text{\AA}$ interval are : Si IV (λ 1394, λ 1403), C II (λ 1335) and C III (λ 1246, λ 1308, λ 1909 and λ 1923). We highlight the presence of several lines between $\sim 1400 - 1900\text{\AA}$. According to our models they stem mainly from Fe IV transitions. Indeed, if we ignore iron, a flat spectrum is produced in this region. Thanks to the high resolution used, the spectrum after $\sim 1850\text{\AA}$ could be matched after the inclusion of Al III, which gave origin to the transitions λ 1855 and λ 1863 ($3p^2P^o - 3s^2S$).

In Fig. 3 we show our model and the high-resolution IUE spectrum in the $\sim 2000 - 3000\text{\AA}$ range. Unfortunately, the signal-noise ratio of this region is not so good, although several lines could be identified : C III (e.g., λ 2010, λ 2092, λ 2163, λ 2296 and λ 2726), C IV (e.g., λ 2405, λ 2524, λ 2530, λ 2698), Ne III (λ 2553 and λ 2678), and two He II lines (λ 2511 and λ 2733). The S V λ 2654 line is indicated in the plot and will be discussed together with the neon lines later in the paper. The 2950 – 3100Å interval presents important features and it was used to derive the oxygen abundance.

4.1.2. Physical parameters and chemical abundances

The basic parameters of our final model are shown in Table 2. In addition, we also show in Table 3 the wind efficiency η ($= \dot{M}v_{\infty}c/L$) and the blanketed ionizing flux shortward of 912Å (Q_o), 504Å (Q_1) and 228Å (Q_2). These values can be useful in future nebular investigations.

There are some differences between our results for BD +30 3639 and the work by Leuenhagen et al. (1996). Their parameters are also in Table 2, and are scaled for the distance of 1.2kpc. Regarding the mass-loss, our value is $5 \times 10^{-7}M_{\odot}/yr$, almost one order of magnitude less than their value, which is $4 \times 10^{-6}M_{\odot}/yr$. Even without clumping our result is significantly lower, $\dot{M}/\sqrt{f} = 1.6 \times 10^{-6}M_{\odot}/yr$. It is important to note that their definitions of star temperature (T_*) and effective temperature (T_{eff}) are different from ours. Our T_{eff} is the temperature where the Rosseland optical depth is 2/3. This temperature is called $T_{2/3}$ in their work and they found 42000K. Our T_* is defined where the Rosseland optical depth is 20. They call it the effective temperature and found 47000K. The reason for quoting two temperatures is that $T_{2/3}$ is often strongly affected by the wind properties.

At first glance, our results are somewhat different from those recently published by Crowther et al. (2006), who also used the CMFGEN code and the same distance ($d = 1.2kpc$) derived by us. It must be kept in mind however that we have adopted throughout this work a fixed value for the luminosity ($L = 5000L_{\odot}$, on the basis of evolutionary results already cited) while their model for BD +30 3639 has $L \sim 6000L_{\odot}$. Our derived T_* differs by about 15% from theirs and our T_{eff} differs by only about 3%. Moreover, their physical parameters have been derived basically from the fitting of the lines C II $\lambda 4267$, C III $\lambda 5696$ and C IV $\lambda\lambda 5801, 5812$, while we have chosen to utilize the whole spectrum. Another reason for the differences found is the slightly different visual magnitude obtained by us, which is $V = -1.3$, as well as a different extinction correction. Given these uncertainties, we conclude that the results shown in Table 2 are not incompatible.

The chemical abundance of the final model is $\beta_{He} = 43\%$, $\beta_C = 51\%$ and $\beta_O = 6\%$ (by mass), which corresponds to $C/He = 0.4$ and $O/He = 0.035$ (by number). In order to test the sensitivity of our models to abundance changes we ran models with different values for C/He, fixing O/He at 0.035. A reasonable range for the C/He ratio in this object is $0.2 \leq C/He \leq 0.6$. The O III lines in the 2950–3100Å interval (see Fig. 3) were used to determine the O/He ratio. In order to check the presence of nitrogen, N II- IV was added during test models. We could not identify any conspicuous transitions in the observed spectra. Using lines such as N III $\lambda 4097$ we can conclude that its abundance is $\beta_N < 0.2\%$.

We were able to estimate a range for the iron abundance of $0.13 \lesssim \beta_{Fe}/\beta_{Fe\odot} < 1$. In Fig.

4 (top) we can see that a solar value results in stronger lines compared to the observations. On the other side, a value of 6% of the solar abundance (bottom) is too low. Our conclusion is that BD +30 3639 shows a deficiency in iron, but the exact value is difficult to determine. Our best fit uses 25% of the solar iron abundance. Similar results were also found in other works (see Miksa et al. 2002 and references therein). These facts support theoretical calculations which predict that iron is depleted by neutron capture occurring during and after the AGB phase (see Herwig et al. 2003; Werner & Herwig 2006). According to Werner & Herwig (2006), some of the iron is converted into nickel and a definite signature of its depletion would be the reduction of the Fe/Ni ratio below the solar value (~ 20), to ~ 3 . We tested models including Ni III-V, but we were unable to determine the nickel abundance precisely. Therefore, the most we can say is that our result favors the expectation that iron is depleted, but a quantitative comparison involving nickel is not possible at present.

4.2. NGC 40

The central star of NGC 40 is classified as [WC8] (Crowther et al. 1998). Its effective temperature is quite controversial. On one hand, Bianchi & Grewing (1987) claimed a value of $\sim 90000K$ from the analysis of UV spectra. With the use of a non LTE expanding atmosphere code, Leuenhagen et al. (1996) derived $T_* \sim 78000K$ and $T_{eff} \sim 46000K$. In contrast to these results, the nebula presents a low excitation class compatible with a central star temperature of only $\sim 38000K$ (Pottasch et al. 2003). Thus, it seems that the nebula does not perceive the central star temperature. Based on these facts, Bianchi & Grewing (1987) proposed the existence of a carbon curtain screening high energy photons. A qualitative UV analysis was also presented by Feibelman (1999), where a terminal velocity of $\sim 1700 \text{ km s}^{-1}$ was derived from the C IV $\lambda 1549$ line. This study also reinforced a high temperature of $\sim 90000K$ by fitting the continuum with a blackbody curve and based on the presence of the stellar He II $\lambda 1640$.

4.2.1. Optical and ultraviolet fit

In Fig. 5 we show our model and the observed optical spectrum. The value derived for the distance is 1.4 kpc. For the interstellar reddening we use an E(B-V) of 0.41. The C III $\lambda 4650$ line is the most intense in the entire spectrum. Other important features are He II $\lambda 4686$, He II $\lambda 5412$, C IV $\lambda 5471$, C III $\lambda 5696$ and C IV $\lambda \lambda 5801, 12$. In contrast to BD +30 3639, where C III dominates, C IV starts to compare in strength with C III and C II is weak (e.g., $\lambda 4267$) or absent. This suggests that NGC 40 has T_{eff} higher than 48000K (BD

+30 3639’s value), in contrast with low values found from nebular techniques (Pottasch et al. 2003). We will see quantitative details in the next section.

Fortunately, FUSE spectra are also available for NGC 40. No quantitative study of the FUSE spectral region has been previously done for this star. The spectrum in the interval 1087–1182Å (LiF2A channel) is shown in Fig. 6 (top) along with our model. Despite having a higher temperature than BD +30 3639, we still had to include P V to fit the features in $\lambda 1118$ and $\lambda 1128$. Other lines identified with the help of our models are C III $\lambda 1175$, C IV $\lambda 1108$ (which might have interstellar absorption lines contaminating it) and C IV $\lambda 1169$.

The fit to the IUE spectrum is also presented in Fig. 6. High-resolution data was used in the $\sim 1000 - 2000\text{\AA}$ interval. Some conspicuous features are : He II $\lambda 1640$, Si IV $\lambda 1722$, C III $\lambda 1909$ and C III $\lambda 1923$. The Si IV $\lambda 1722$ and S V $\lambda 1502$ lines will be discussed in Section 5.

We did not get a very good fit to C IV $\lambda 1549$ even using a Voigt profile. Difficulties in the fitting of this feature have already been reported before and it is known that this line is very sensitive to clumping (Hillier & Miller 1999; Crowther et al. 2002). However, a decrease of the filling factor f from 0.1 to 0.03 improves the fit, but only regarding its intensity. A very low value of 0.01 was tried, but is not so different from the 0.03 fit and it is probably too extreme. With a lower mass-loss we can get a better profile, but we have a drawback regarding the fit quality in other parts of the spectrum. The reduced mass-loss improves the fit since it reduces the optical depth of C IV $\lambda 1549$. The optical depth in this line is large, and as a consequence the Voigt wings are important for the formation of the observed profiles. The neglect of partial redistribution effects, which might be significant in such a case, is likely to contribute to the discrepancy.

A low resolution IUE spectrum was used in the $\sim 2000 - 3000\text{\AA}$ range (bottom of Fig. 6). The C III $\lambda 2296$ theoretical line is too strong. Unfortunately, changes of the model parameters do not lead to better agreement without adversely affecting the fit to other features. The remaining transitions present a very reasonable fit.

4.2.2. *Physical parameters and chemical abundances*

The parameters for NGC 40 are shown in Table 2. Scaling the results of Leuenhagen et al. (1996) to our distance, we find : $R_* = 0.46R_\odot$, $L = 7450L_\odot$ and $\dot{M} = 4 \times 10^{-6}M_\odot/yr$. Their higher luminosity is reflected in their higher value for T_* . As for BD +30 3639, our derived mass loss rate (\dot{M}/\sqrt{f}) is approximately a factor of 2 lower than that found using the Potsdam model.

As mentioned earlier, the temperature of NGC 40 is controversial. On the one hand, nebular techniques such as the Zanstra and Stoy method provide a temperature around $38000K$ (Pottasch et al. 2003). On the other hand, analysis of the central star seems to indicate temperatures up to $\sim 90000K$. In order to address this issue, we ran several models with different effective temperatures. From the response of optical and UV lines (e.g., C IV $\lambda 1549$, C III $\lambda 4650$, He II $\lambda 4686$, C III $\lambda 5696$ and C IV $\lambda \lambda 5801, 12$) to temperature changes, we conclude that NGC 40 has $T_{eff} = (71 \pm 10)kK$. A possible reason for the low central star temperatures found by nebular techniques is the neglect of a stellar wind and the use of the black-body approximation. The number of ionizing photons emerging to the planetary nebula can deviate significantly from that of the inner parts of the stellar wind. This can result in a planetary nebula perceiving the central star as a low temperature object. For example, for a star with $T_* = 38000K$ which radiates like a black-body (BB), the number of ionizing photons per second are $\text{Log } Q_0^{BB} = 47.37$, $\text{Log } Q_1^{BB} = 46.33$ and $\text{Log } Q_2^{BB} = 43$. Our results, for $T_* \sim 73kK$ are : $\text{Log } Q_0 = 47.56$, $\text{Log } Q_1 = 46.91$ and $\text{Log } Q_2 = 36.79$. As can be seen, our values for H I and He I are compatible with the BB values and for He II our model indicates a much lower number of photons. Therefore, the number of ionizing photons escaping from the wind is consistent with (or even less than) the number of ionizing photons of a star with a much lower temperature, if it radiates like a black-body (as assumed in some nebular methods). A consistent analysis of the wind and the nebula, with the stellar parameters obtained here as input parameters on a photoionization model will certainly help clarify this problem.

The chemical abundance of the final model is $\beta_{He} = 43\%$, $\beta_C = 51\%$ and $\beta_O = 6\%$ (by mass), which corresponds to $C/He = 0.40$ and $O/He = 0.035$ (by number). Decreasing C/He below this value improves the fits to He II $\lambda 5412$ and C IV $\lambda 5471$, but C III $\lambda 5696$ starts to get too weak. Our uncertainty estimate for C/He is the same as for BD +30 3639, i.e., $0.2 \leq C/He \leq 0.6$. We used O III $\lambda 5593$ and the O III lines in the $2950 - 3100\text{\AA}$ interval as the diagnostic lines for the determination of the O/He ratio. Nitrogen features are not observed in this object. If present, its abundance in mass fraction is $\beta_N < 0.1\%$ and it does not influence the spectrum. By including N III–V we could verify for example, that N IV $\lambda 1718$ appeared and it does not exist in the IUE spectrum. Regarding iron, it is difficult to say if this object has an abundance lower than solar. An ultraviolet synthetic spectrum in the $1000 - 2000\text{\AA}$ region with a solar iron abundance is not different enough from a lower value ($\sim 80\%$ less) to allow a firm conclusion.

4.3. NGC 5315

NGC 5315 is classified as a [WC4] star by Crowther et al. (1998) and as a [WO4] star by Acker & Neiner (2003). The planetary nebula is compact ($\sim 4''$), almost spherical and was studied from the infrared to the ultraviolet (see for example, Pottasch et al. 2002 and Peimbert et al. 2004). So far, no spectroscopic analysis of the central star has been performed using a non LTE code. Feibelman (1998) presented a qualitative analysis based on IUE data and obtained a terminal velocity of 3600 km s^{-1} and $T_* \sim 80000K$. de Freitas Pacheco et al. (1986; 1993) derived $T_* \sim 82700K$ and a terminal velocity of 2600 km s^{-1} . However, Pottasch et al. (2002) claim a lower temperature of $\sim 66000K$ based on the Zanstra method for hydrogen and on the absence of He II lines in the nebula. As we mentioned previously, nebular methods that assume black-body radiation from [WR] stars should not be used to derive their temperatures.

4.3.1. Optical and ultraviolet fit

Early-type [WR] stars usually have intense mass-losses and high terminal velocities ($v_\infty \sim 1000 - 3500 \text{ km s}^{-1}$). The latter complicates their modeling because many spectral features are severely blended. We highlight in particular the $\lambda 4650$ and $\lambda 5805$ features seen in Fig. 7, where we compare the synthetic and observed spectrum. According to our model, the feature at $\lambda 4650$ is composed of He II, C III and C IV, whilst $\lambda 5805$ is pure C IV. The distance used is 2.5kpc and the interstellar reddening is $E(B-V) = 0.37$ (Pottasch et al. 2002).

The far-ultraviolet fit to the FUSE spectrum is shown in Fig. 8 (top). Again, we highlight the presence of the P V lines $\lambda 1118$ and $\lambda 1128$. The fit presented uses four times the solar phosphorus abundance and it will be discussed further in Section 5. The transitions C III $\lambda 1175$ and C IV $\lambda 1108$ and $\lambda 1169$ could also be identified.

For the UV analysis we used low resolution IUE spectra. Our fit is shown in Fig. 8. The most intense lines are indicated in the plot. The observed spectrum in the $\sim 2000 - 3000\text{\AA}$ interval was obtained in the IUE small aperture mode and it was scaled by a factor of 2.5. We decided not to use the other available large aperture spectra because they seem to show nebular continuum contamination beyond 2500\AA . The compactness of the planetary nebula and the large aperture of $10'' \times 20''$ support this idea. Unfortunately, the signal-noise ratio in $\sim 2000 - 3000\text{\AA}$ is not so good. Nevertheless, our model allowed us to identify the presence of C IV $\lambda 2405$, C IV $\lambda 2530$ and C III $\lambda 2296$. Feibelman (1998) considered this last feature as having a nebular origin, but our fit suggests otherwise.

4.3.2. Physical parameters and chemical abundances

The parameters of our final model for NGC 5315 are shown in Table 2. If compared to de Freitas Pacheco et al. (1986; 1993), our unclumped mass-loss is virtually the same. However, their radius and luminosity ($L = 3924L_{\odot}$) are different, implying a higher T_* . It is interesting to note that the majority of the early-type WR stars analyzed so far have T_* in the range $\sim 120 - 150kK$ (see Koesterke 2001). Regarding six LMC WC4 (Pop. I) stars and using CMFGEN, Crowther et al. (2002) found on average $T_* \sim 87kK$ and $T_{eff} \sim 70kK$, more in line with our values. This point will be discussed further in Section 5.

The parameters obtained are not so different from those of NGC 40, which is a [WCL]. The very different spectral appearance in this case relies on the terminal velocity, which is 1000 km s^{-1} for NGC 40. Values up to 3600 km s^{-1} as determined by Feibelman (1998) were tested and are too high, making several features much broader than the observed.

The adopted final chemical abundance is : $\beta_{He} = 43\%$, $\beta_C = 51\%$ and $\beta_O = 6\%$ (by mass), which corresponds to $C/He = 0.40$ and $O/He = 0.035$ (by number). This result will be discussed further in Section 5. For the determination of O/He we used the $\lambda 5595$ feature, which is due to O III $\lambda 5592$ and some O V transitions that have $\lambda 5598$ as the main contributor. Again, no trace of nitrogen was found in the observed spectra. If present, its abundance is $\beta_N < 0.1\%$ and it does not produce any conspicuous transitions.

Regarding iron, we could see an improvement in the fit of the region $1400 - 1500\text{\AA}$ using an abundance lower than solar. This is shown in Fig. 9. We estimate the following range for this object : $0.1 \lesssim \beta_{Fe}/\beta_{Fe_{\odot}} < 1$. This is another result supporting iron depletion by neutron capture occurring during and after the AGB phase. As in the case of BD +30 3639, we could not obtain a reliable value for the Fe/Ni ratio. For NGC 5315, the inclusion of nickel did not produce visible transitions in the spectrum.

4.4. NGC 6905

NGC 6905 is the hottest central star of our sample. Crowther et al. (1998) assign a [WO1] classification for this object while the [WO2] type is preferred by Acker & Neiner (2003). These two classes represent the highest ionization stages among [WR] stars. This is readily seen in its spectrum through intense and broad emission lines of O VI, C IV and He II.

The first spectroscopic study of this object, based on non LTE expanding atmosphere models, was presented by Koesterke & Hamann (1997b). Again, line-blanketing and clump-

ing were not considered. Peña et al. (1998) extended this work by analyzing the planetary nebula through a photoionization code. With the stellar model ionizing flux as an input parameter, the ionization structure and electronic temperature of the nebula were reproduced reasonably well, but some important discrepancies remained. For example, the $H\beta$ theoretical flux obtained was less than observed, which suggests the need for better central star parameter estimates and up to date physics.

The IUE spectra of NGC 6905 were studied qualitatively by Feibelman (1996). Several useful line identifications and flux measurements from both low and high dispersion spectra were presented and two high terminal velocities were derived : 3800 km s^{-1} from C IV $\lambda 1549$ and 2700 km s^{-1} from O V $\lambda 1371$.

4.4.1. *Optical and ultraviolet fit*

In Fig. 10 we present the observed and theoretical optical spectra. The derived distance and reddening are $d = 1.75 \text{ kpc}$ and $E(B-V) = 0.20$. An important transition in this region is O VI $\lambda\lambda 3811, 34$. Previous early-type [WR] models had difficulty reproducing the strength of this line, generally predicting a profile weaker than observed by a factor of ~ 2 (see Peña et al. 1998). The fit achieved by us, although somewhat weaker than the observed, it is reasonable and it results from our compromise with other O VI lines and O V $\lambda 1371$ regarding temperature changes. The feature in $\sim 4660 \text{ \AA}$ results from added contributions of C IV (mainly $\lambda 4658$ and $\lambda 4684$) and He II ($\lambda 4686$). Other less intense lines are : O VI $\lambda 5291$, He II $\lambda 5412$, C IV $\lambda 5471$ and C IV $\lambda\lambda 5801, 12$. Contrary to the other stars in this work, given its high temperature, NGC 6905 does not present C III.

In Fig. 11 (top) we present the far-ultraviolet fit to the FUSE spectra. We identified : O VI $\lambda\lambda 1032, 38, \lambda 1081$ and $\lambda 1125$ and C IV $\lambda 1108$ and $\lambda 1169$. The oxygen lines were used together with O V $\lambda 1371$ to constrain the effective temperature. In order to better fit the continuum, a slightly lower value for $E(B-V)$ of 0.15 had to be used.

We used low resolution IUE spectra for the $\sim 1000 - 3000 \text{ \AA}$ interval. Our fit is also shown in Fig. 11. Between $1200 - 2000 \text{ \AA}$ we have three stellar lines : O V $\lambda 1371$, C IV $\lambda 1549$ and He II $\lambda 1640$. Helium lines are usually well reproduced in our models, but clearly this is not the case of He II $\lambda 1640$. This line has a contamination by the nebula and as Feibelman (1996) highlighted, its intensity might change with the position angle of the IUE aperture. The remaining feature, at 1909 \AA , is a nebular C III semi-forbidden transition.

We found some differences between the predicted and observed spectrum in the $2000 - 3000 \text{ \AA}$ interval. The only theoretical lines that get close to the observed ones are O VI $\lambda 2070$,

C IV $\lambda 2529$ and $\lambda 2905$. Feibelman (1996) claimed that several lines in this IUE region are due to Fe II, O III, [Ar V], [Mg V] and [Ne IV- V]. Taking into account that Fe II and O III transitions are not seen in our models (due to the high temperature) and that some features are related to forbidden transitions, we suggest that at least part of the discrepancies seen have a nebular origin. Lines from highly ionized elements such as C V, C VI, O VII and O VIII (not included in our models) might also contribute to the emissions in this region. They are present in the spectrum of some [WR] stars and also in some PG 1159 stars and DO white dwarfs (see for example Koesterke & Hamann 1997a).

We considered the possibility that an enhanced neon abundance could fit the emission near 2200\AA . An oversolar amount of this element is expected from evolutionary calculations and was indeed necessary to fit the spectra of some CSPN (Herald et al. 2005). We tested neon abundances up to $10\times$ the solar value and the resultant Ne VI lines did not have the right wavelengths to adequately match the observed profile. We emphasize that this is not the only unidentified emission in the spectrum of NGC 6905. In the optical for example, our model could not reproduce a weak, broad emission at 4920\AA . A similar stellar feature at $\sim 2200\text{\AA}$, which also remains unidentified, is seen in the spectrum of the hot, massive star Sand 2 (Crowther et al. 2000).

4.4.2. *Physical parameters and chemical abundances*

The physical parameters of our final model can be found in Table 2. Compared to NGC 5315, NGC 6905 is hotter (approximately a factor of 2), and has both a smaller radius and a denser wind. Although they both are early-type [WR] stars, their spectral appearances are quite distinct. NGC 5315 still presents C III and O VI is weak or absent, whilst C IV and O VI are dominant in NGC 6905. Regarding the temperature, Koesterke & Hamann (1997b) found $\sim 141kK$ and our value is $\sim 150kK$. As no particular distance is adopted in their work, we are only able to compare the transformed radius R_T , which they found to be $\sim 3R_\odot$ while we found $\sim 5R_\odot$ without clumping.

Our final model has the following chemical abundances : $\beta_{He} = 49\%$, $\beta_C = 40\%$ and $\beta_O = 10\%$ (by mass), which corresponds to $C/He = 0.27$ and $O/He = 0.05$ (by number). This result will be discussed in the next section. Regarding nitrogen, no conspicuous transitions can be seen in the observed spectra. We estimate an upper limit of $\beta_N < 0.1\%$.

Because this object is very hot, we included the dominant ionization stages of iron, which are Fe VII–VIII. Some subtle changes can be seen in the FUSE region with a lower iron abundance (e.g., 1/10 of the solar value) but they are not enough to determine whether

there is a deficiency or not.

5. Discussion

5.1. C/He mass ratios of the early-type [WR] stars

It is claimed that for early-type [WR] stars the C/He mass ratio (β_C/β_{He}) is considerably smaller than in other classes ([WCL], [WELS] and PG 1159). In Table 4 we show the average mass fractions of He, C and O for all H deficient central stars analyzed so far. The range of values measured by atmosphere models is shown for each element. This problem was first mentioned by Koesterke & Hamann (1997a,b) and contradicts the evolutionary sequence, because early-type [WR] stars are supposed to be descendents of the [WCL] stars. Furthermore, β_C/β_{He} is expected to be about unity from stellar evolution models regardless which thermal pulse (AFTP, LTP or VLTP) is responsible for the hydrogen deficiency (Herwig 2001). It is still unclear if such a discrepancy is due to effects not taken into account in older models (e.g., line-blanketing).

The determination of β_{He} and β_C is usually based on the transitions He II $\lambda 5412$ and C IV $\lambda 5471$. These lines are adopted since both are formed by recombination in a similar region of the stellar wind. In Fig. 12 we have a spectral interval comprising these two lines for the two early-type stars of our sample, NGC 5315 and NGC 6905, respectively. In order to investigate the low β_C/β_{He} issue found in previous works, we plot two models along with the observations : one with $\beta_C/\beta_{He} \sim 0.35$, which is the average value found for the early-type [WR] stars, and another with this ratio approaching unity. For NGC 5315, none of the models present a reasonable fit to these lines. We also tested lower values for β_C and β_{He} at the expense of an increase in β_O . Although the fit showed a better quality, some oxygen lines increased considerably (e.g., O III- V $\lambda 5595$). In the case of NGC 6905, a β_C/β_{He} ratio of ~ 0.8 is better than ~ 0.35 (bottom panel). This lower value is essentially the same as that adopted by Koesterke & Hamann (1997). The ratio of ~ 0.8 is more in line with values found in other classes (see Table 4) and with what is expected from evolutionary calculations. It is very important to note however, that the fits are not perfect. The determination of the continuum and a He II $\lambda 5412$ nebular contamination (as is clear from the figure for NGC 6905) are factors that can complicate the analysis. At least from our results, it is not clear if early-type [WR] stars have smaller β_C/β_{He} ratios. A larger sample of objects with better signal-noise spectra should be carefully analyzed. In doing so, we should keep in mind a commitment with other parts of the spectrum when fitting He II $\lambda 5412$ and C IV $\lambda 5471$.

5.2. Silicon, phosphorus, sulfur and neon abundances

The silicon features present in the spectra of [WR] stars deserve special attention. Stellar evolution models predict that silicon has essentially a solar mass-fraction in the H-He intershell matter in AGB stars. As a consequence, we expect to measure roughly a solar value, i.e., $\beta_{Si} \sim 0.07\%$, when analyzing H-deficient CSPN (see Werner & Herwig 2006 and references therein). However, Leuenhagen & Hamann (1998) derived $\beta_{Si} = 0.5 - 3\%$ in a couple of [WCL] stars. These mass fractions correspond to 7 to 40 times the solar value, indicating a huge discrepancy with theory. Motivated by this, we used silicon lines in the spectra of BD +30 3639 and NGC 40 in order to check if the same high over solar abundances would be found. It turned out that the transitions Si IV $\lambda 1722$ in NGC 40 and Si IV $\lambda 1394$, $\lambda 1403$ and $\lambda 4089$ in BD +30 3639 were well reproduced using a solar silicon abundance. Despite an uncertainty of approximately a factor of two in our determination, our results are in agreement with stellar evolution models. As reported by Werner & Herwig (2006), near solar values were also found in a few PG 1159 stars.

The atomic model for silicon used in the work of Leuenhagen & Hamann (1998) was relatively simple (see their table 1). Moreover, neither clumping nor metal line-blanketing was taken into account in their study. Therefore, it would be interesting to re-analyze the stars in their sample in order to check if more sophisticated models could influence the silicon abundance determination. This could confirm or nullify the conflict with stellar evolution models.

Thanks to the FUSE spectra available for all stars in our sample, we could identify phosphorus in the spectrum of BD +30 3639, NGC 40 and NGC 5315. The 1100 – 1130Å interval could only be fitted after the inclusion of P V, which gave origin to the transitions $\lambda 1118$ and $\lambda 1128$ ($3p^2P^o - 3s^2S$). From nucleosynthesis calculations, phosphorus is expected to be observed with 4 – 25 times the solar abundance, depending on the treatment of convective mixing (Werner & Herwig 2006). In fact, the NGC 5315 spectrum could be better matched using abundances in this range. On the other hand, BD +30 3639 and NGC 40 models were too insensitive to changes in the phosphorus abundance for a reliable abundance to be derived. They allow not only over solar values in the expected range but also a solar abundance. Hence, we can say that the result for NGC 5315 supports nucleosynthesis predictions, while for the other two stars the error in the abundance determination is too large to draw any conclusions.

Evolutionary calculations predict that sulfur should be observed with an abundance of 0.6 – 0.9 of the solar value (Werner & Herwig 2006). We searched for sulfur lines in the spectra of each star of our sample. In all objects they are very weak or undetectable. From our models, we found that the following lines can be used as diagnostics for the abundance

determination : S V $\lambda 1502$, S V $\lambda 2654$, and S IV $\lambda 3107$. For BD +30 3639 we estimate an upper limit of $\beta_S \lesssim \beta_{S_\odot}$, in agreement with what is expected from stellar evolution models. For NGC 40 and NGC 5315, a higher limit was adopted, namely, $\beta_S \lesssim 2\beta_{S_\odot}$. We could not estimate the sulfur abundance in NGC 6905. Given its high temperature, S VI is fully ionized throughout its stellar wind and we currently lack S VII atomic data.

Neon is expected to be overabundant in hydrogen deficient CSPN. According to Werner & Herwig (2006), its mass fraction should be $\sim 2\%$, i.e., about 10 times the solar value, although slightly lower or higher values are predicted depending on the initial mass of the star. In our models, neon diagnostic lines were found in the 2000-3000Å interval. For NGC 40 and NGC 5315, the IUE spectra in this region have low resolution, limiting the accuracy of the analysis. No conspicuous neon transitions are seen. From the lines Ne IV $\lambda 2364$, Ne III $\lambda 2553$ and Ne III $\lambda 2678$, we estimate a rough upper limit of ~ 8 times the solar neon value. For NGC 6905, by using the theoretical transitions Ne VI $\lambda 2641$ and Ne VI $\lambda 2687$ we estimate an upper limit of 5 times the solar neon value. Higher abundances make these lines much stronger than observed.

In contrast to the other stars, BD +30 3639 present neon lines in the near UV. Although the IUE spectrum in the 2000-3000Å region does not have a good signal-noise ratio, we can identify Ne III $\lambda 2553$ and Ne III $\lambda 2678$ (see Fig. 3). With a solar neon abundance, this last transition is practically absent in the models. We could only have a reasonable agreement with the observed Ne III $\lambda 2678$ line by using a neon mass fraction of $\sim 2\%$. Therefore, BD +30 3639 is the only case in our sample that definitely support the prediction of stellar evolution models.

5.3. Evolutionary sequence

A comparison among our results and previous works that did not include line-blanketing and clumping can be seen in Fig. 13. In this diagram, the suggested evolution is to decrease the transformed radius while the temperature increases when going from the [WCL] to the early-type [WR] stars. This would be the result of a shrinking radius and higher mass-loss. As we get near the white dwarf phase, i.e., shortly afterwards the [WELS] and PG 1159 stage, a wind shut down is expected (Koesterke & Werner 1998). The abrupt decrease in mass-loss rate increases the transformed radius. At the same time, regarding the spectra, the number of absorptions starts to overwhelm the number of emission lines. From our results, we can conclude that :

- The inclusion of clumping in [WR] models can change the $R_T \times T_*$ diagram in Fig.

13 considerably. If clumping is present in all [WR] stars in a uniform way, i.e., if they can be described by the same filling factor f , the mass-losses will be diminished by a factor of ~ 3 (for $f = 0.1$). Thus, we will have a vertical shift of the same amount for each star because the transformed radius is inversely proportional to $\dot{M}^{2/3}$:

$$R_T = R_* \left(\frac{v_\infty/2500 \text{ km s}^{-1}}{\dot{M}/10^{-4} M_\odot \text{ yr}^{-1}} \right)^{2/3} .$$

Among the analyzed stars, direct evidence for clumping is shown only for BD +30 3639 and NGC 40.

- Compared to previous homogeneous models, the transformed radii increase to ~ 0.5 dex. Without clumping, we still found a change of $\sim 0.1 - 0.2$ dex.
- Our result for NGC 6905 suggests that the gap found between early-type [WR] stars and [WELS] could disappear if clumping is not important or present in this latter group.
- A far-UV to optical coverage plus the use of line-blanketing is probably the reason for the change in the temperatures of all stars regarding previous results. However, we did not see any systematic change that would allow any conclusion regarding the evolutionary sequence. We decreased the temperatures of NGC 40 and NGC 5315 and increased the temperatures of NGC 6905 and BD +30 3639. An important case to note is the one of NGC 5315, which will be discussed in the next section. This star is clearly far from the other early-type objects. An analysis of a larger sample is required to check if the same behavior can be found.

Fig. 13 allows us to check the differences between our work and previous results. However, it is interesting to compare our results also with evolutionary tracks in the HR diagram. Indeed, this kind of comparison was one of the strongest arguments first supporting an evolutionary connection between [WR], [WELS] and PG 1159 stars (see Hamann 1997). Unfortunately, there are some drawbacks in doing this. First, the radii determined from the models are distant dependent whilst Fig. 13 is not. Hence, the determination of surface gravities can be very uncertain. Absorption lines in PG 1159 stars are used to overcome this difficulty, but the same is not possible for the [WR] stars. Another concern are the evolutionary tracks. Generally, the ones used are tailored for H-rich objects, which could be another source of uncertainty. The main reason for this is the complexities involved in getting a H-deficient object and its evolution in an appropriate way. Nevertheless, very recently, Althaus et al. (2005) made available a complete evolutionary track for a $2.7 M_\odot$ star from

the main sequence up to the normal (H-rich) white dwarf stage. Further, after a very late thermal pulse (VLTP), the calculations were carried out to the H-deficient PG 1159 stage and finally, to the DO, DB and DQ white dwarf region. Their work fits our needs and is reproduced here in our Fig. 14. The number of data points are augmented by our analysis and by new results regarding PG 1159 stars (Hügelmeier et al. 2005). We also add to the plot all the previously analyzed Galactic [WR] stars (Koesterke 2001). All [WR] stars are assumed to have $0.6M_{\odot}$. Although the [WR] \rightarrow PG 1159 evolution can be inferred from Fig. 14 (based on an appropriate evolutionary track), some remarks should be made :

- There is not a smooth transition from [WCL] to the early-type [WR] stars (see $\text{Log } T_* > 4.9$). This reflects the long standing issue regarding the lack of stars in the subtypes [WC5-7], i.e., there are no [WR] stars with T_* between $\sim 80kK$ and $\sim 110kK$;
- NGC 5315 ([WC4]-[WO4]) is clearly displaced from other early-type [WR] stars. The majority of early-type [WR] stars are distributed over a very narrow region near the PG 1159 stars, where $T_* > 100kK$. In contrast, the position of NGC 5315 is practically the same as NGC 40, which is a [WCL] star. It must be kept in mind that although some early-type [WR] and PG 1159 stars occupy a region in common in this diagram (near $\text{Log } g = 6$), their spectra are quite distinct. In contrast with PG 1159 stars, all early-type [WR] stars present mass-loss;
- As already noted by Hamann (1997), the position of [WELS] in Fig. 14 is slightly before the early-type [WR] stars. This is another point showing the need for the analysis of more objects in this class.

Until we elucidate the points described above, the detailed evolutionary sequence [WCL] \rightarrow [WCE] \rightarrow [WO] \rightarrow [WELS] \rightarrow PG 1159 must be considered with caution.

It would be very useful to have the same diagram but for the other two thermal pulse models (AFTP and LTP) and for different remnant stellar masses. This is beyond the scope of the present work.

5.4. The early-type [WR] star NGC 5315

As already mentioned, the T_* found for NGC 5315 is lower than previous determinations for other [WC4] stars, namely : IC 1747, NGC 1501 and NGC 6369 (see Koesterke 2001). However, it is important to note that they all now have different stellar classifications. Recently, because some [WCE] stars present oxygen lines more intense than carbon lines,

new classification systems (Crowther et al. 1998; Acker & Neiner 2003) replaced [WC2-3] by [WO1-4] subtypes, changing the status of several objects (including some [WC4]) and giving a more appropriate description of the ionization of the wind. It turns out that NGC 5315 now is the only object analyzed from its class, which according to Crowther et al. (1998) is [WC4] and to Acker & Neiner (2003), [WO4]. As a matter of fact, NGC 5315 is clearly separated from other early-type [WR] stars in the diagrams in Figs. 13 and 14. This result should not be interpreted as the influence of the use of metal line-blanketing, and calls for an analysis of more objects in the [WC4]-[WO4] class.

6. Summary

We presented detailed far-UV to optical analysis of four [WR] stars. New physical parameters and abundances for the central stars BD +30 3639, NGC 40, NGC 5315 and NGC 6905 were obtained using CMFGEN. Contrary to most of the previous works about these objects, metal line-blanketing and a simple treatment of clumping were taken into account. The early-type [WR] star NGC 5315 was studied for the first time by means of non LTE expanding atmosphere models. So far, no other object from its spectral class ([WC4]-[WO4]) has been analyzed with a similar code.

Far-UV FUSE observations of all stars were analyzed for the first time. Phosphorus was found in the spectra of BD +30 3639, NGC 40 and NGC 5315. The transitions $\lambda 1118$ and $\lambda 1128$ could be identified as P V ($3p^2P^o - 3s^2S$). Regarding its abundance, the result for NGC 5315 agrees with nucleosynthesis calculations during the AGB phase, where a range of 4 – 25 times the solar value is predicted. For the other objects, the models were too insensitive to abundance changes and a solar value is also possible.

We derived a solar silicon abundance for two stars of our sample : BD +30 3639 and NGC 40. Although we estimate an uncertainty of a factor of two in this determination, our result is in agreement with the prediction that the silicon abundance should not show a significant deviation from the solar value.

We estimated upper limits for the amount of sulfur in BD +30 3639, NGC 40 and NGC 5315. Regarding neon, upper limits for its abundance were established for NGC 40, NGC 5315 and NGC 6905. In order to provide a reasonable fit to the Ne III $\lambda 2678$ line in BD +30 3639, we used a neon abundance of $\sim 2\%$ (mass fraction). This result supports the prediction of an oversolar neon abundance in hydrogen deficient CSPN.

An analysis of the iron abundance was performed for each star. Evidence of depletion was found for BD +30 3639 and NGC 5315, while for the other stars, the spectrum was not

sensitive enough to iron abundance changes to allow a reliable estimate. The confirmation of a depletion supports theoretical calculations based on neutron capture during and after the AGB phase. A parallel confirmation of iron depletion through the enrichment of nickel could not be achieved for BD +30 3639 and NGC 5315. At present, it is very difficult to determine a reliable abundance for this element.

Using the results for NGC 5315 and NGC 6905, we addressed the issue of the low C/He mass ratios of the early-type [WR] stars. We had difficulties in obtaining a simultaneous fit of He II $\lambda 5412$ and C IV $\lambda 5471$ in the models for NGC 5315. Neither the typical low value of $\beta_C/\beta_{He} \sim 0.35$ found in previous works or $\beta_C/\beta_{He} \sim 1$ was able to satisfactorily reproduce these lines. For NGC 6905, a value of $\beta_C/\beta_{He} \sim 0.8$ is better than a lower one and it is more compatible with values found in the other classes. For a more reliable analysis, we need spectra with good flux calibrations and high S/N. In this way, we can better determine the stellar continuum, better measure the strengths and profiles of weak features, and better separate the nebular contamination.

The impact of our results on the evolutionary sequence [WR] \rightarrow PG 1159 is shown in the transformed radius-temperature and HR diagrams. The latter made use of the evolutionary track of Althaus et al. (2005), which is suitable for H-deficient objects. Although there are displacements regarding previous results in these diagrams due to the new physics added (e.g., metal line-blanketing and clumping), a deeper comprehension of the evolution of these stars requires the investigation of a larger sample. In particular, an analysis of more stars of the [WELS] class and of other early-type [WR] stars with the same spectral classification as NGC 5315 is desirable.

W. M. thanks Fundação de Amparo à Pesquisa do Estado do Rio de Janeiro (FAPERJ) for financial support. DJH gratefully acknowledges partial support from NASA LTSA grant NAG5-8211.

REFERENCES

- Acker, A., Grosdidier, Y., & Durand, S., 1997, *A&A*, 317, L51
- Acker, A., & Neiner, C., 2003, *A&A*, 403, 659
- Althaus, L. G., Serenelli, A. M., Panei, J. A., Córscico, A. H., García-Berro, E., & Scóccola, C. G., 2005, *A&A*, 435, 631
- Arnaud, K., Borkowski, K. J., & Harrington, J. P., 1996, *ApJ*, 462, L75

- Bachiller, R., Forveille, T., Huggins, P. J., Cox, P., & Maillard, J. P., 2000, *A&A*, 353, L5
- Bianchi, L., & Grewing, M., 1987, *A&A*, 181, 85
- Blöcker, T., 2001, *Ap&SS*, 275, 1
- Bouret, J. -C., Lanz, T., & Hillier, D. J., 2005, *A&A*, 438, 301
- Crowther, P. A., De Marco, O., & Barlow, M. J., 1998, *MNRAS*, 296, 367
- Crowther, P. A., Dessart, L., Hillier, D. J., Abbott, J. B., & Fullerton, A. W., 2002, *A&A*, 392, 653
- Crowther, P. A., Morris, P. W., & Smith, J. D., 2006, *ApJ*, 636, 1033
- Crowther, P. A., et al., 2000, *ApJ*, 538, L51
- de Araújo, F. X. de , Marcolino, W. L. F., Pereira, C. B., & Cuisinier, F., 2002, *AJ*, 124, 464
- de Freitas Pacheco, J. A., Codina, S. J., & Viadana, L., 1986, *MNRAS*, 220, 107
- de Freitas Pacheco, J. A., Costa, R. D. D., de Araújo, F. X., & Petrini, D., 1993, *MNRAS*, 260, 401
- De Marco, O., & Barlow, M. J., 2001, *Ap&SS*, 275, 53
- De Marco, O., & Crowther, P. A., 1998, *MNRAS*, 296, 419
- De Marco, O., & Crowther, P. A., 1999, *MNRAS*, 306, 931
- De Marco, O., & Soker, N., 2002, *PASP*, 114, 602
- Dessart, L., & Hillier, D. J., 2005, *A&A*, 439, 671
- Dreizler, S., & Heber, U., 1998, *A&A*, 334, 618
- Feibelman, W. A., 1996, *ApJ*, 472, 294
- Feibelman, W. A., 1998, *ApJ*, 506, 773
- Feibelman, W. A., 1999, *ApJ*, 514, 296
- Gorny, S. K., & Tylenda, R., 2000, *A&A*, 362, 1008
- Gräfener, G., Koesterke, L., & Hamann, W. -R., 2002, *A&A*, 387, 244

- Grosdidier, Y., Acker, A., & Moffat, A. F. J., 2000, *A&A*, 364, 597
- Grosdidier, Y., Acker, A., & Moffat, A. F. J., 2001, *A&A*, 370, 513
- Hamann, W. -R., 1997, in *Proc. IAU Symp. 180*, ed. H. J. Habing, & H. J. G. L. M. Lamers (Kluwer), 91
- Harrington, J. P., Lane, N. J., White, S. M., & Borkowski, K. J., 1997, *AJ*, 113, 2147
- Herald, J. E., & Bianchi, L., 2004a, *ApJ*, 609, 378
- Herald, J. E., & Bianchi, L., 2004b, *ApJ*, 611, 294
- Herald, J. E., & Bianchi, L., Hillier, D. J., 2005, *ApJ*, 627, 424
- Herwig, F., 2001, *Ap&SS*, 275, 15
- Herwig, F., Lugaro, M., & Werner, K., 2003 in *Planetary Nebulae, Proc. of IAU Symp. 209*, ed. S. Kwok, M. Dopita, & R. Sutherland, 85
- Hillier, D. J., & Miller, D. L., 1998, *ApJ*, 496, 407
- Hillier, D. J., & Miller, D. L., 1999, *ApJ*, 519, 354
- Hügelmeier, S. D., Dreizler, S., Werner, K., Krzesiński, Nitta, A., & Kleinman, S. J., 2005, *A&A*, 442, 309
- Iben, I., Kaler, J. B., Truran, J. W., & Renzini, A., 1983, *ApJ* 264, 605
- Kastner, J. H., Soker, N., Vrtilik, S. D., & Dgani, R., 2000, *ApJ*, 545, L57
- Maness, H. L., Vrtilik, S. D., Kastner, J. H., & Soker, N., 2003, *ApJ*, 589, 439
- Koesterke, L., 2001, *Ap&SS*, 275, 41
- Koesterke, L., & Hamann, W. -R., 1997a, *A&A*, 320, 91
- Koesterke, L., & Hamann, W. -R., 1997b, in *Planetary Nebulae, Proc. of IAU Symp. 180*, ed. H. J. Habing, & H. J. G. L. M. Lamers, 114
- Koesterke, L., & Werner, K., 1998, *ApJL*, 500, L55
- Kruk, J. W., & Werner, K., 1998, *ApJ*, 502, 858
- Leuenhagen, U., & Hamann, W. -R., 1998, *A&A*, 330, 265

- Leuenhagen, U., Hamann, W. -R., & Jeffery, C. S., 1996, *A&A*, 312, 167
- Li, J., Harrington, J. P., & Borkowski, K. J., 2002, *AJ*, 123, 2676
- Marcolino, W. L. F., & de Araújo, F. X., 2003, *AJ*, 126, 887
- Miksa, S., Deetjen, J. L., Dreizler, S., Kruk, J. W., Rauch, T., & Werner, K., 2002, *A&A*, 389, 953
- Owocki, S. P., 1994, *Ap&SS*, 221, 3
- Parthasarathy, M., Acker, A., & Stenholm, B., 1998, *A&A*, 329, L9
- Peimbert, M., Peimbert, A., Ruiz, M. T., & Esteban, C., 2004, *ApJSS*, 150, 431
- Peña, M., Stasinska, G., Esteban, C., Koesterke, L., Medina, S., & Kingsburgh, R., 1998, *A&A*, 337, 866
- Peña, M., Hamann, W.-R., Ruiz, M. T., Peimbert, A., & Peimbert, M., 2004, 419, 583
- Peña, M., Medina, S., & Stasinska, G., 2003a, *RevMexAA*, 15, 38
- Peña, M., Medina, S., & Stasinska, G., 2003b, *RevMexAA*, 18, 84
- Peña, M., Stasinska, G., & Medina, S., 2001, *A&A*, 367, 983
- Pottasch, S. R., Beintema, D. A., Bernard-Salas, J., Koornneef, J., & Feibelman, W. A., 2002, *A&A*, 393, 285
- Pottasch, S. R., Bernard-Salas, J., Beintema, D. A., & Feibelman, W. A., 2003, *A&A*, 409, 599
- Reiff, E., Rauch, T., Werner, K., & Kruk, J. W., 2005, in *ASP Conf. Series 334, White Dwarfs*, ed. D. Koester, & S. Moehler (San Francisco: ASP), 225
- Schmutz, W., Hamann, W.-R., & Wessolowski, U., 1989, *A&A*, 210, 236
- Stasinska, G., Gräfener, G., Peña, M., Hamann, W. -R., Koesterke, L., & Szczerba, R., 2004, *A&A*, 413, 329
- Tylenda, R., Acker, A., & Stenholm, B., 1993, *A&AS*, 102, 595
- Waters, L. B. F. M., Beintema, D. A., Zijlstra, A. A., Koter, A. de, Molster, F. J., Bouwman, J., Jong, T de., Pottasch, S. R., & Graauw, Th. de, 1998, *A&A*, 331, L61

Werner, K., & Heber, U., 1991b, *A&A*, 247, 476

Werner, K., Heber, U., & Hunger, K., 1991a, *A&A*, 244, 437

Werner, K., & Herwig, F., 2006, *PASP*, 118, 183

Zijlstra, A. A., van Hoof, P. A. M., Chapman, J. M., & Loup, C., 1994, *A&A*, 290, 228

Table 1: Atomic Model for BD +30 3639.

Ion	Number of full levels	Number of super-levels
He I	39	27
He II	30	13
C II	338	104
C III	243	99
C IV	64	49
O II	111	30
O III	349	267
O IV	72	30
O V	91	31
O VI	19	13
Ne II	48	14
Ne III	71	23
Ne IV	52	17
Mg II	45	18
Al II	58	38
Al III	45	17
Si II	80	52
Si III	45	25
Si IV	38	27
P V	62	16
S III	14	11
S IV	23	19
S V	22	21
S VI	19	17
Ar III	36	10
Ar IV	61	19
Ar V	36	18
Ca II	46	17
Ca III	110	33
Ca IV	193	34
Ca V	121	45
Ca VI	108	47
Fe III	477	61
Fe IV	1000	100
Fe V	182	19
Fe VI	80	10

Note. — NGC 40 and NGC 5315 have practically the same atomic model, the only difference being the number of super-levels in a few ions. For NGC 6905, C II, O II- III, Ne II, Si II, S III and Ca II were excluded, while Ne V- VI, Mg III, Si V and Fe VII- VIII were included.

Table 2: Basic parameters derived and comparison with previous results.

Star	T_* (K)	R_*/R_\odot	T_{eff} (K)	$\log M$	$\log M/\sqrt{f}$	v_∞ (km s $^{-1}$)	R_T/R_\odot	β_{He}	β_C	β_O	d (kpc)
BD +30 3639 (this work)	48060	1.0	46720	-6.30	-5.80	700	6.8 (14.6)	43	51	6	1.2
Leuenhagen et al. (1996)	47000	1.49	42000	-	-5.40	700	5.5 (-)	45	50	5	
Crowther et al. (2006)	55000	0.85	48000	-6.05	-5.55	700	3.9 (8.5)	51	38	10	
NGC 40 (this work)	73310	0.43	70840	-6.25	-5.75	1000	3.4 (7.4)	43	51	6	1.4
Leuenhagen et al. (1996)	78000	0.46	46000	-	-5.40	1000	2.2 (-)	40	50	10	
NGC 5315 (this work)	76420	0.40	74590	-6.33	-5.83	2400	6.5 (13.9)	43	51	6	2.5
de Freitas Pacheco et al. (1986;1993)	82700	0.31	-	-	-5.83	2600	5.2 (-)	-	-	-	
NGC 6905 (this work)	149600	0.10	146200	-7.15	-6.65	1890	4.9 (10.5)	49	40	10	1.75
Koesterke & Hamann (1997)	141000	-	-	-	-	1800	3.4 (-)	60	25	15	

Note. — Mass loss unit is M_\odot year $^{-1}$. Values between parentheses use clumping. Chemical abundances are given in mass fractions. The distances were derived from the models.

Table 3: Additional physical parameters of our models.

Star	Log Q_0 912Å (H I)	Log Q_1 504Å (He I)	Log Q_2 228Å (He II)	η
BD +30 3639	47.45	45.89	34.28	11.0 (3.5)
NGC 40	47.56	46.91	36.79	17.6 (5.5)
NGC 5315	47.58	47.15	37.46	35.6 (11.0)
NGC 6905	47.43	47.30	46.65	4.1 (1.3)

Note. — The ionizing flux unit is $photons\ s^{-1}$ and the values between parentheses for the wind efficiency η use clumping.

Table 4: Average mass fractions for H deficient CSPN.

Class	$\bar{\beta}_{He}$ (%)	$\bar{\beta}_C$ (%)	$\bar{\beta}_O$ (%)	$\bar{\beta}_C/\bar{\beta}_{He}$
[WCL] (13)	43 ± 3	50 ± 4	6 ± 3	1.16 ± 0.12
[WCE] (11)	66 ± 9	23 ± 6	11 ± 4	0.35 ± 0.10
[WELS] (3)	40 ± 7	44 ± 5	14 ± 2	1.10 ± 0.23
PG 1159 (13)	50 ± 17	39 ± 14	10 ± 6	0.78 ± 0.39

Note. — Data from Koesterke (2001); Reiff et al. (2005); Dreizler & Heber (1998); Kruk & Werner (1998). The number of objects considered in each class is between parentheses. Hybrid PG 1159 stars were omitted.

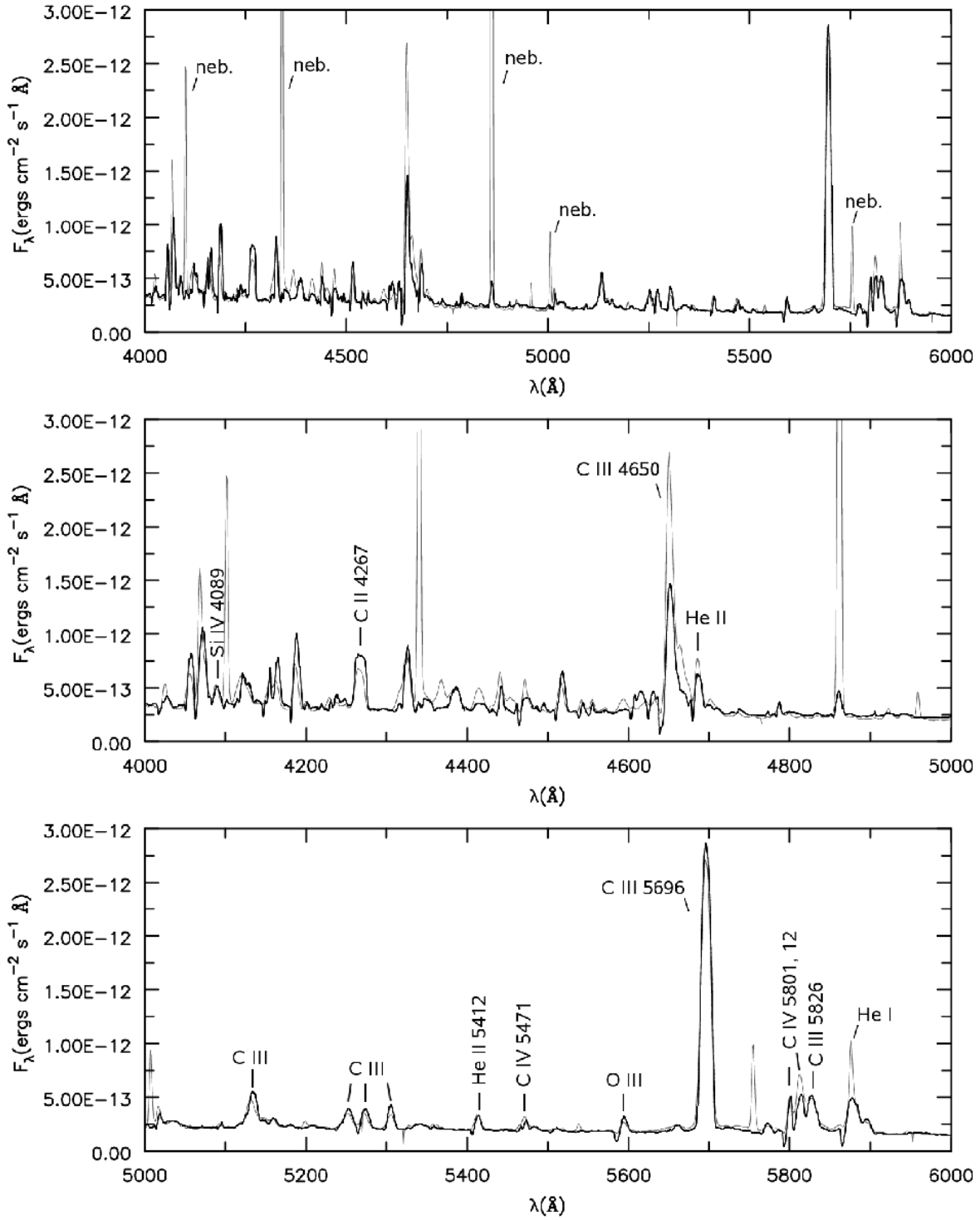


Fig. 1.— BD +30 3639 optical spectrum and our model (thick line). Some nebular lines are indicated in the top panel and identified as : H δ , H γ , H β , [O III] λ 5007 and [N II] λ 5754.

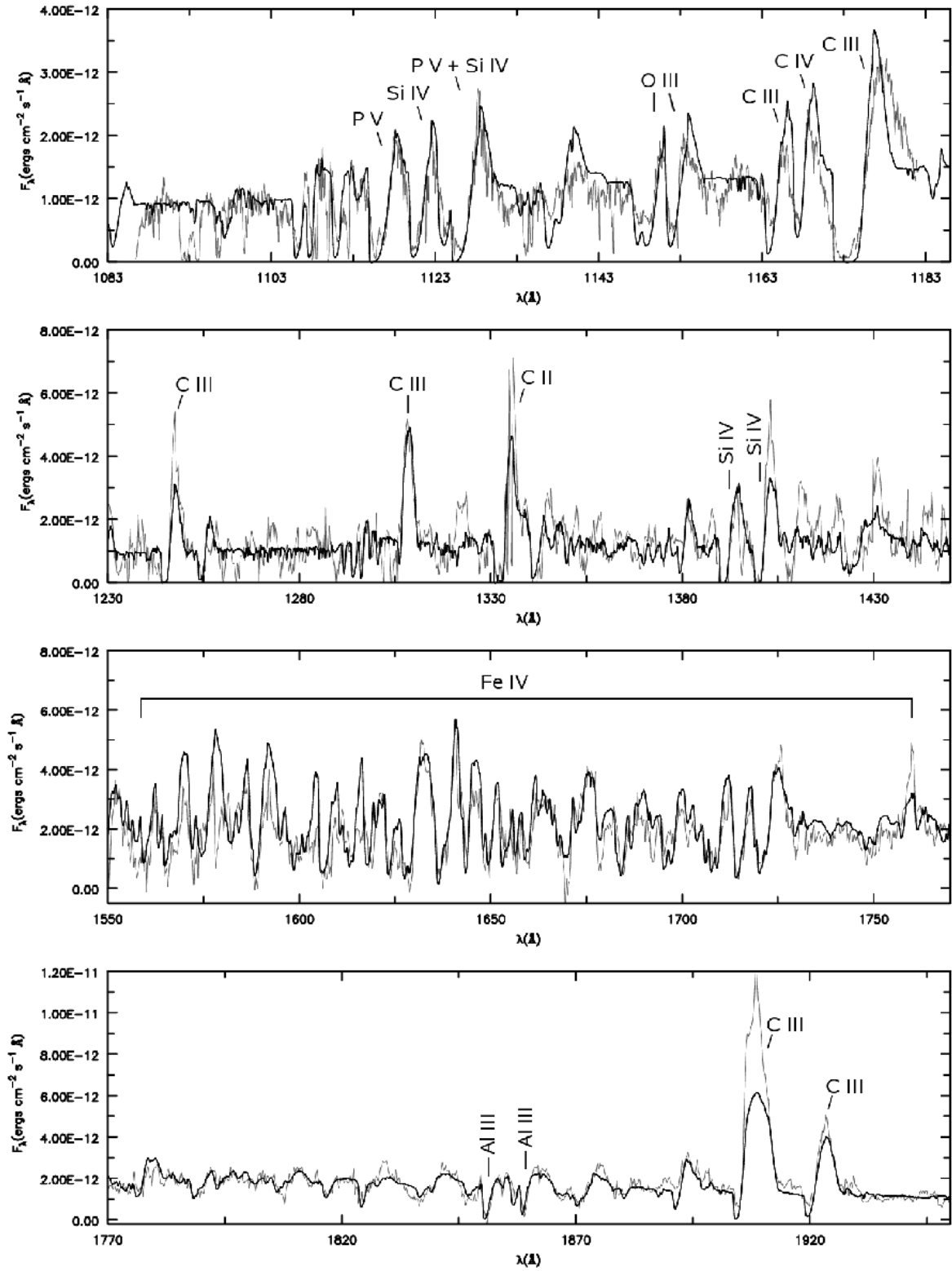


Fig. 2.— BD +30 3639 ultraviolet spectra and our model (thick line). Top : FUSE spectrum. Other Panels : High resolution IUE spectrum.

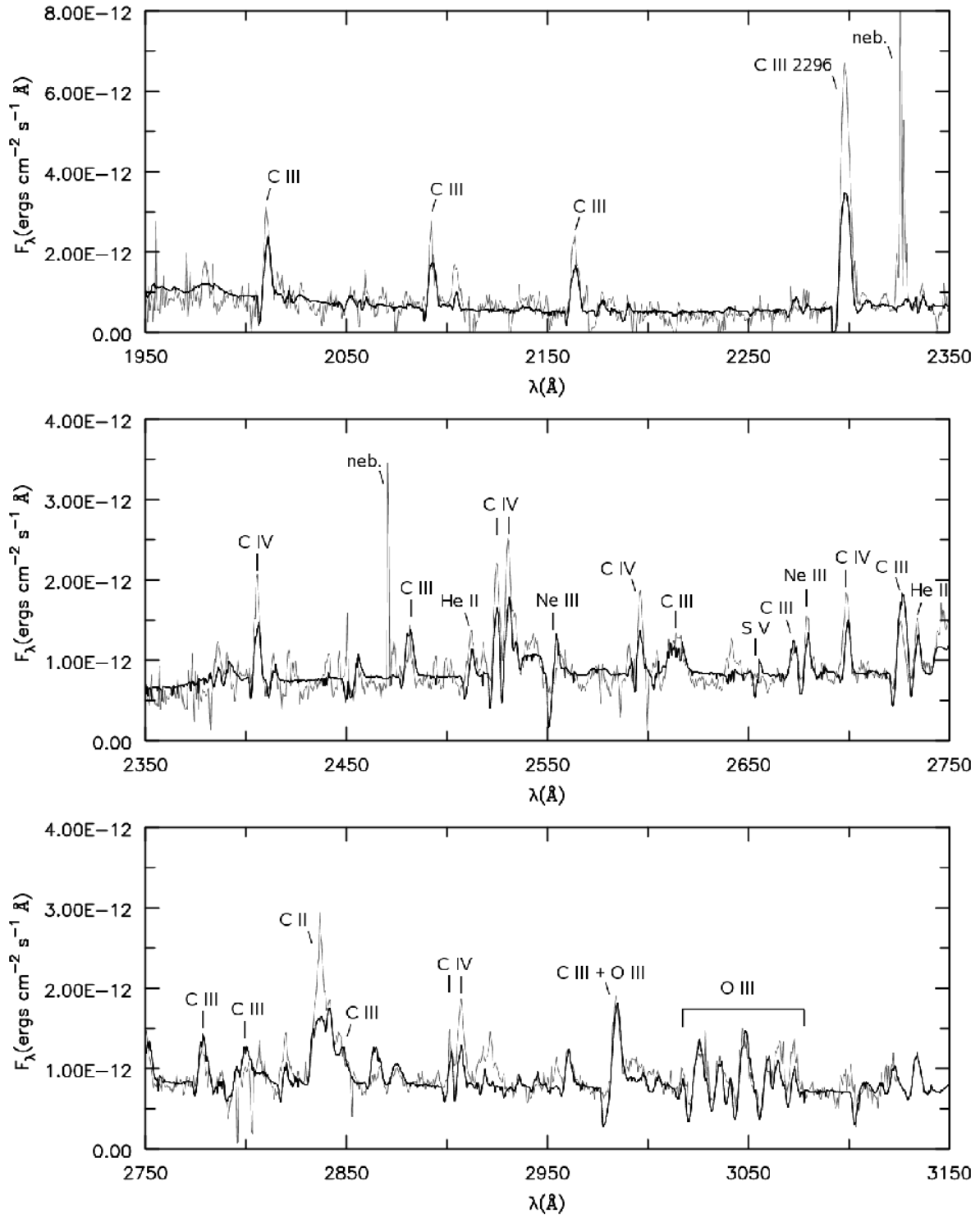


Fig. 3.— BD +30 3639 high resolution UV spectrum and our model (thick line). The nebular lines beyond 2296 \AA are : C II] (λ 2323, λ 2325, λ 2327, λ 2328) and [O II] λ 2471.

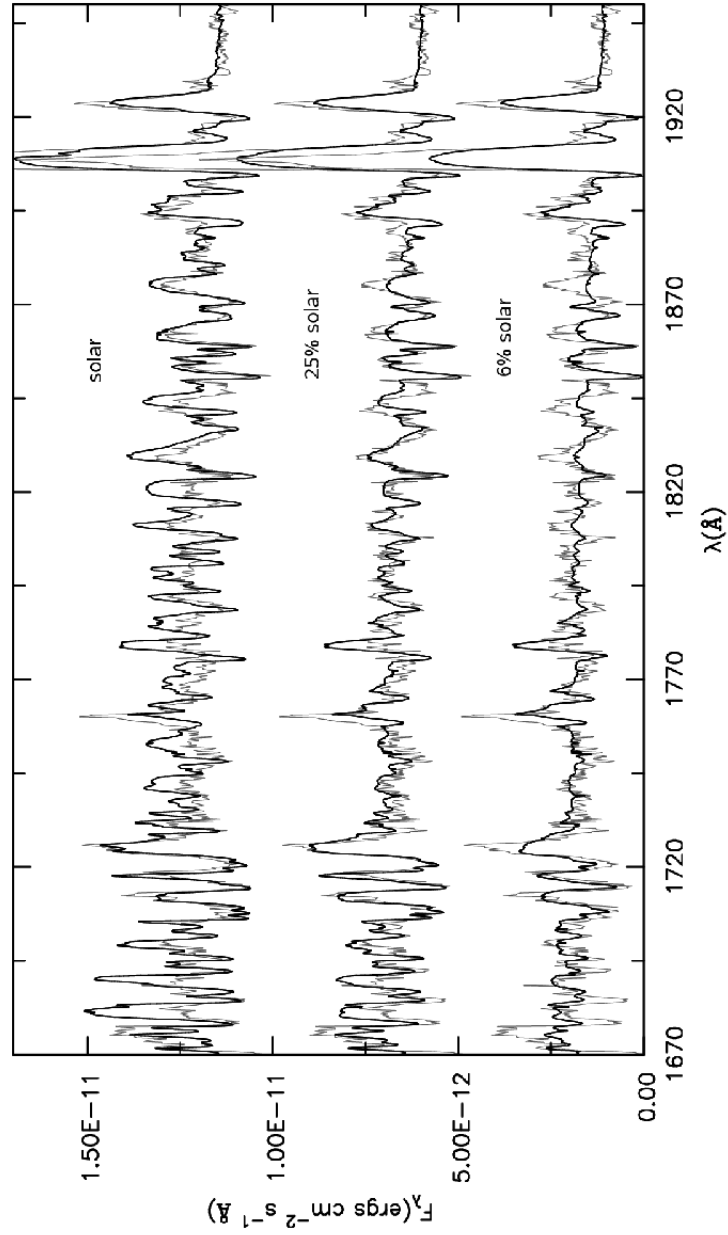


Fig. 4.— Iron deficiency in BD +30 3639. Models are represented by thick lines. Top : solar abundance. Middle : best fit model with 25% of the solar abundance. Bottom : 6% of the solar abundance. The two upper models were vertically displaced for clarity. Abundances are in mass fractions.

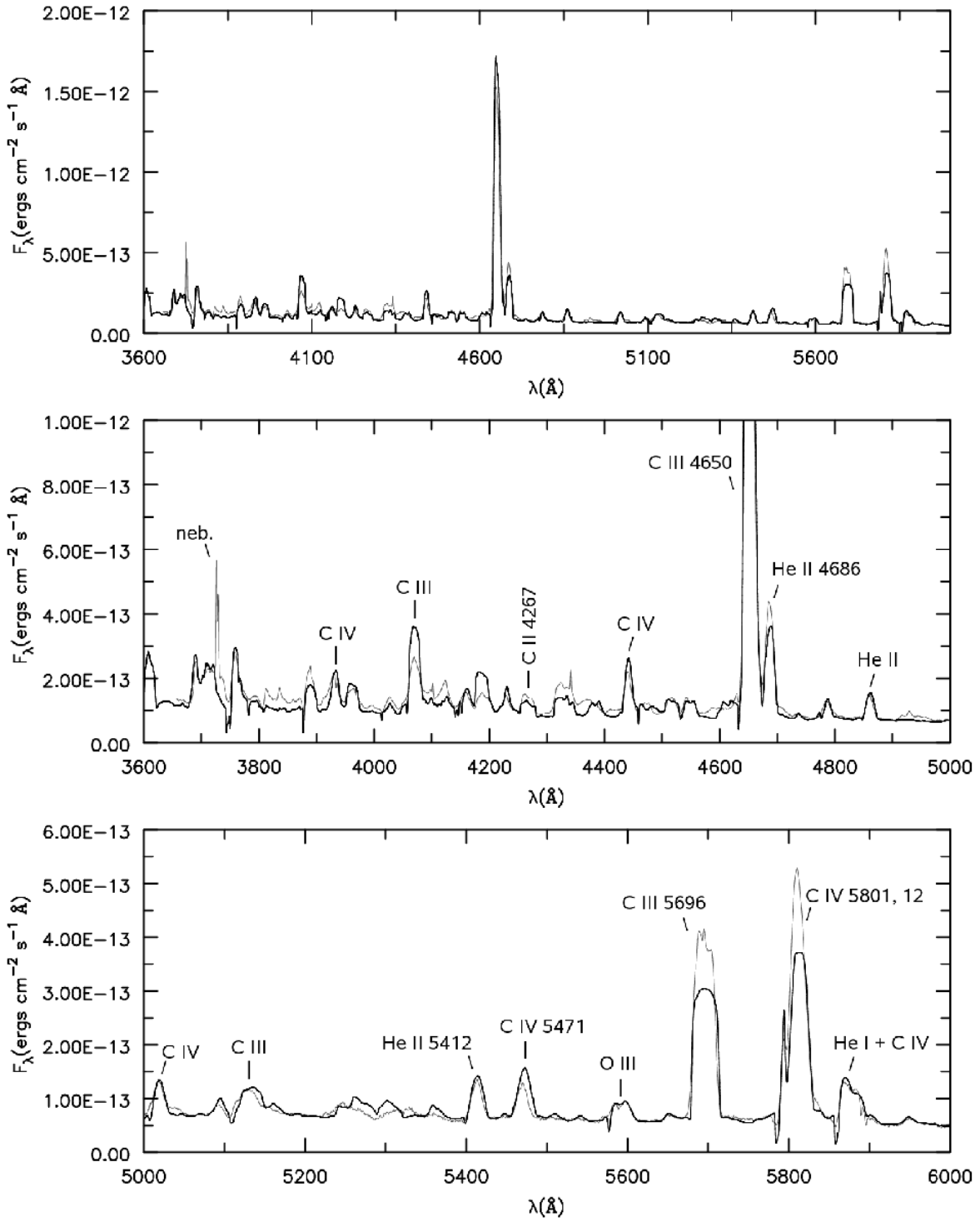


Fig. 5.— NGC 40 optical spectrum and our model (thick line).

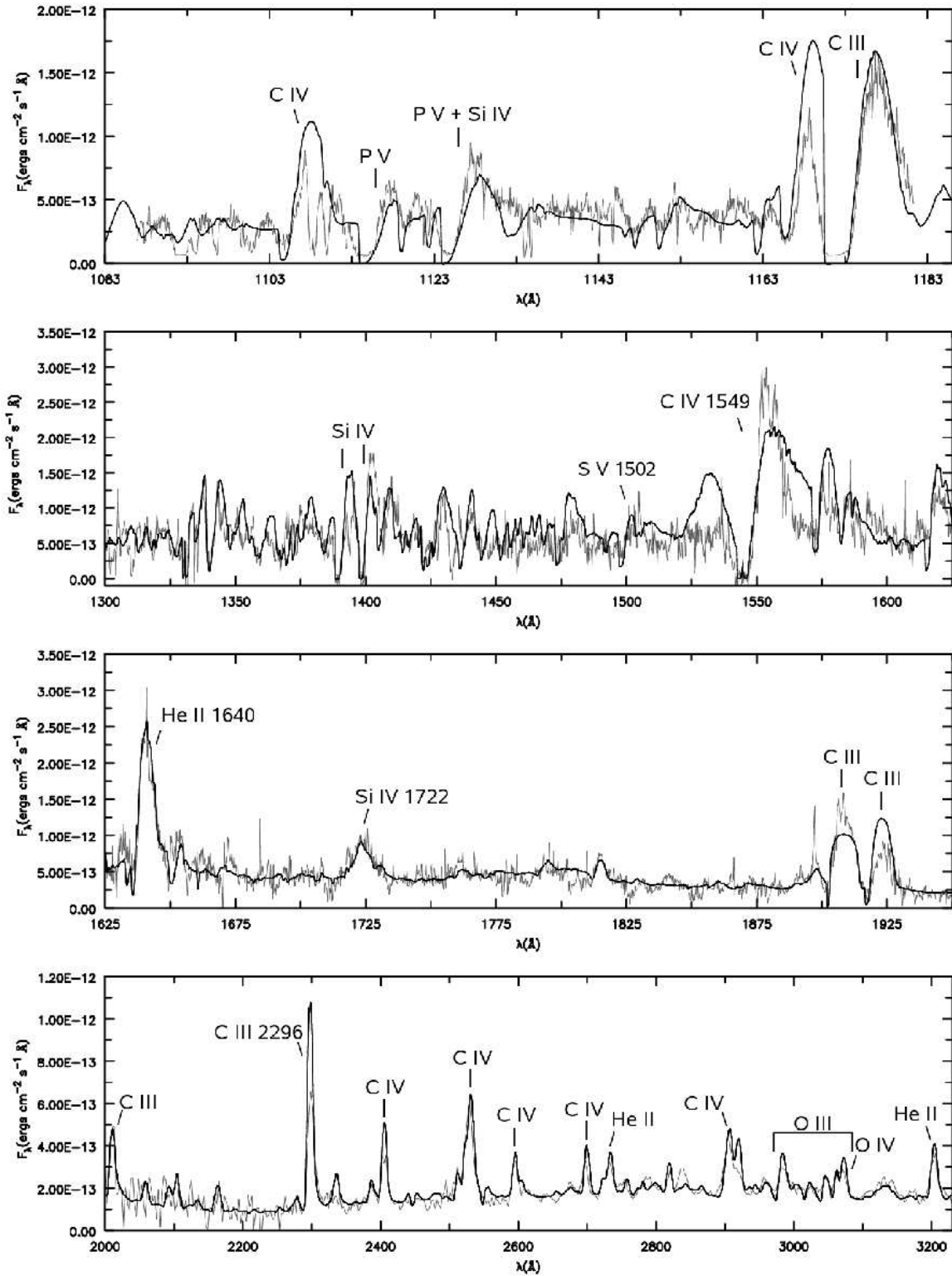


Fig. 6.— NGC 40 ultraviolet spectra and our model (thick line). Top : FUSE spectrum. 2nd and 3rd panel : high resolution IUE spectrum. Bottom : low resolution IUE spectrum.

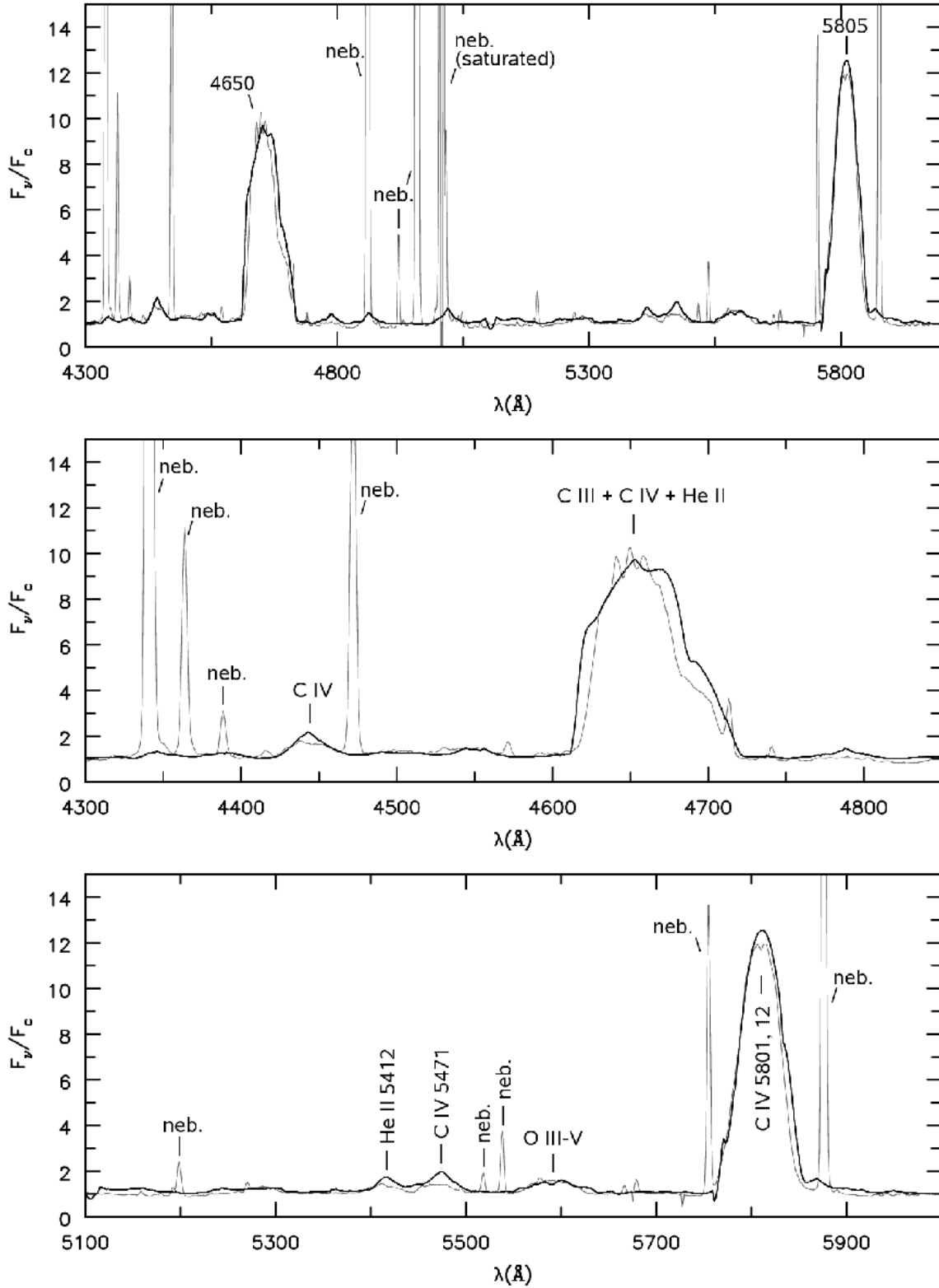


Fig. 7.— NGC 5315 optical spectrum and our model (thick line). The nebular lines are : $H\gamma$, [O III] $\lambda 4363$, He I $\lambda 4388$, $\lambda 4472$, $H\beta$, [O III] $\lambda 4959$, $\lambda 5007$, [N I] $\lambda 5199$, [Cl III] $\lambda 5518$, $\lambda 5538$, [N II] $\lambda 5754$ and He I $\lambda 5876$.

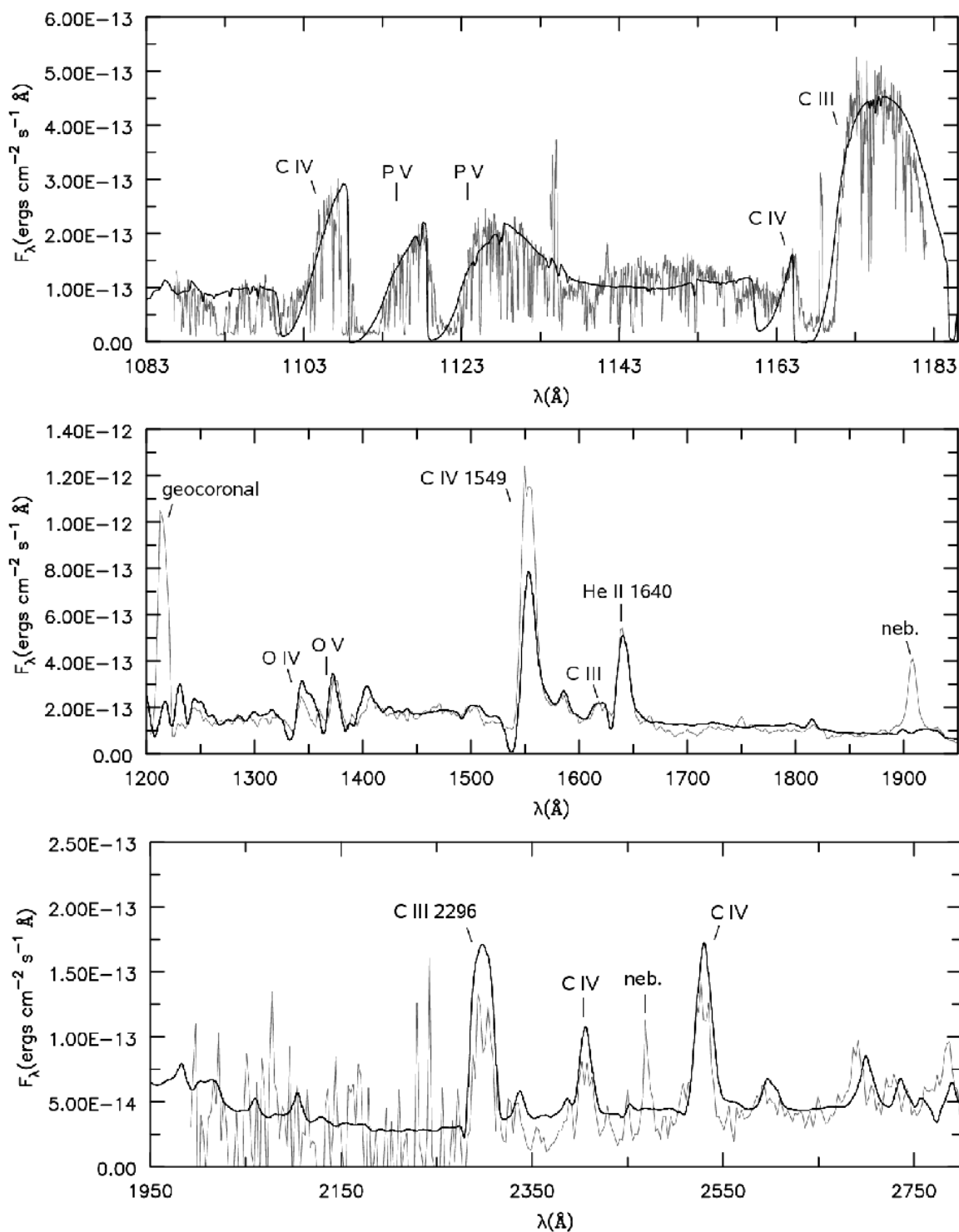


Fig. 8.— NGC 5315 ultraviolet spectra and our model (thick line). Top : FUSE spectrum. Other panels : Low resolution IUE spectra. The non-stellar lines indicated are : $L\alpha$ (geocoronal emission), C III] $\lambda 1909$ and [O II] $\lambda 2470$ (nebular). Unusually, the observed C IV profile lacks the strong P-Cygni absorption generally associated with this line.

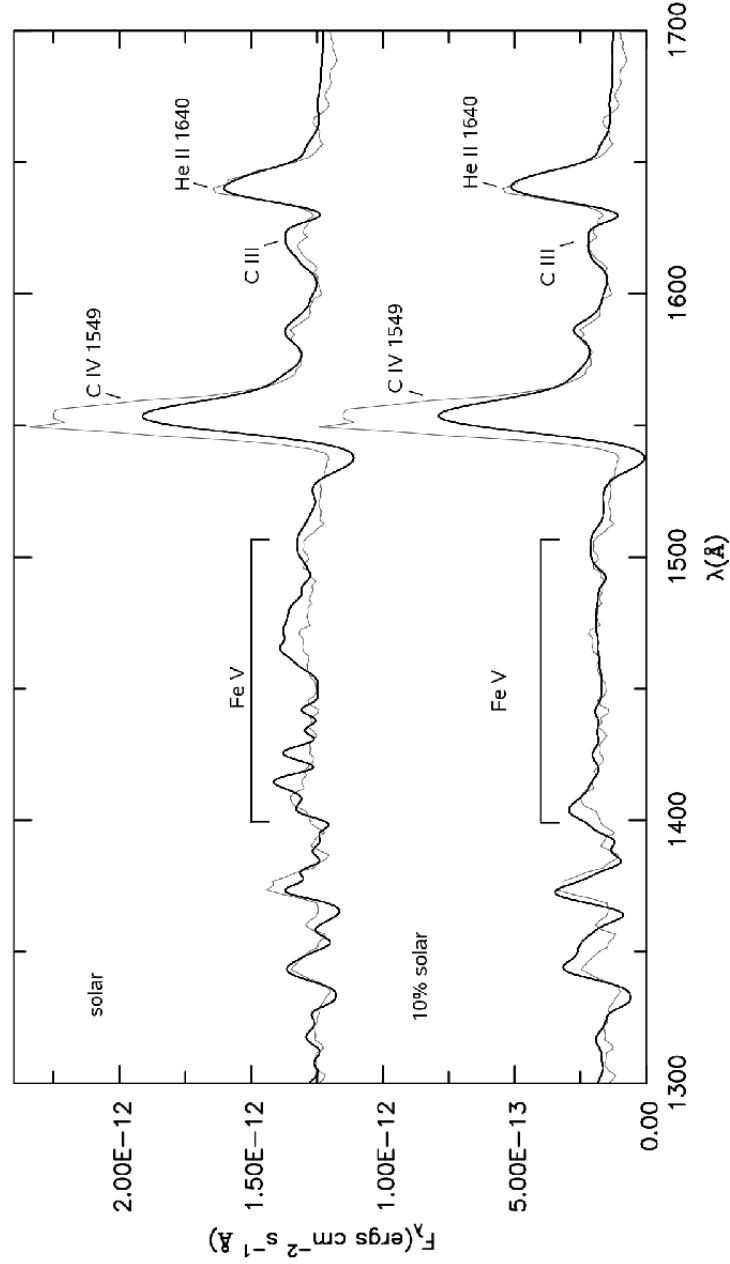


Fig. 9.— Iron deficiency in NGC 5315. Models are represented by thick lines. Top : solar abundance. Bottom : 10% of the solar abundance. The upper model was vertically displaced for clarity. Abundances are in mass fractions.

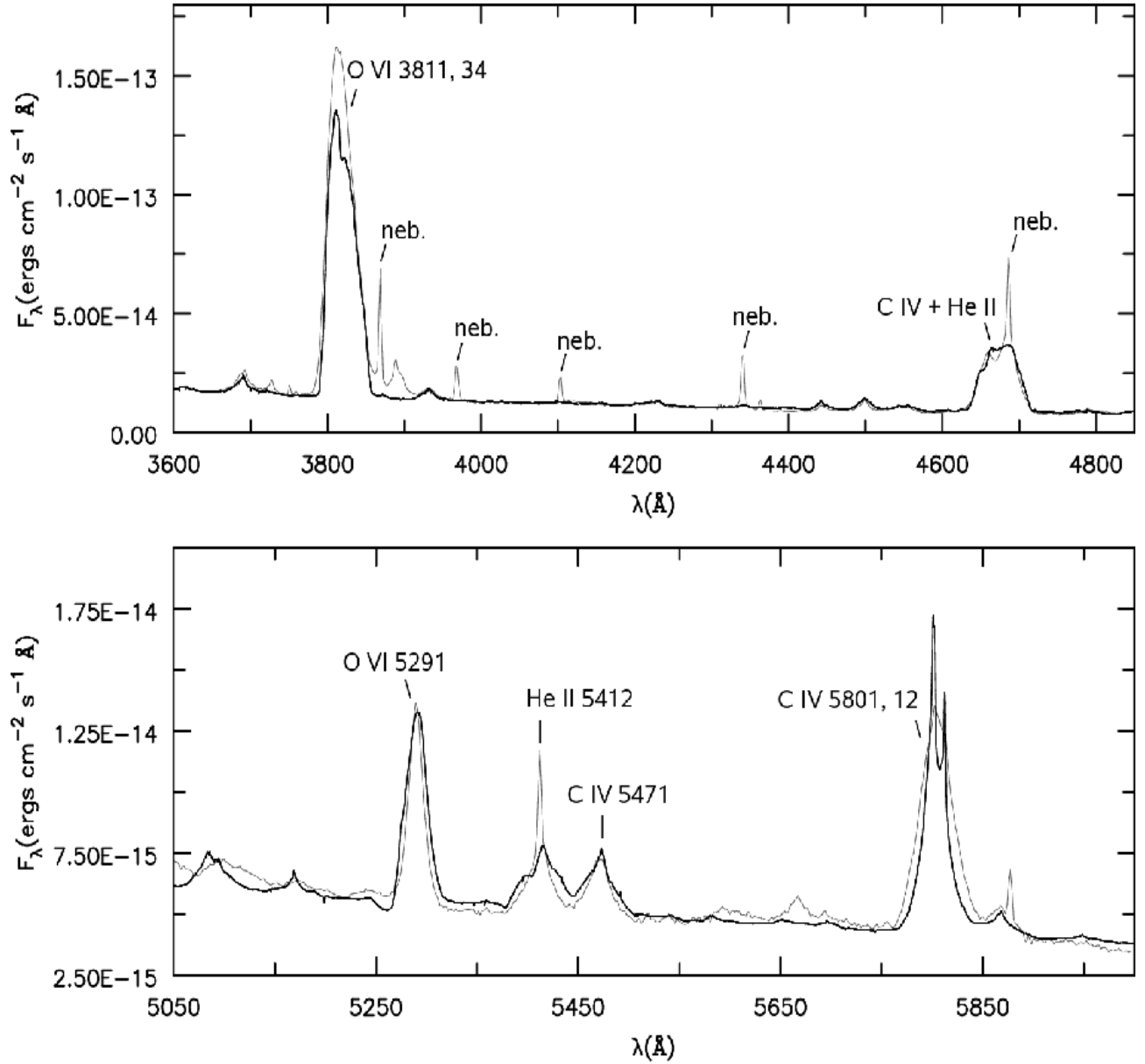


Fig. 10.— NGC 6905 optical spectrum and our model (thick line). Nebular lines are : [Ne III] $\lambda 3868$, $\lambda 3969$, $H\delta$, $H\gamma$, He II $\lambda 4686$ and He II $\lambda 5412$ (contamination).

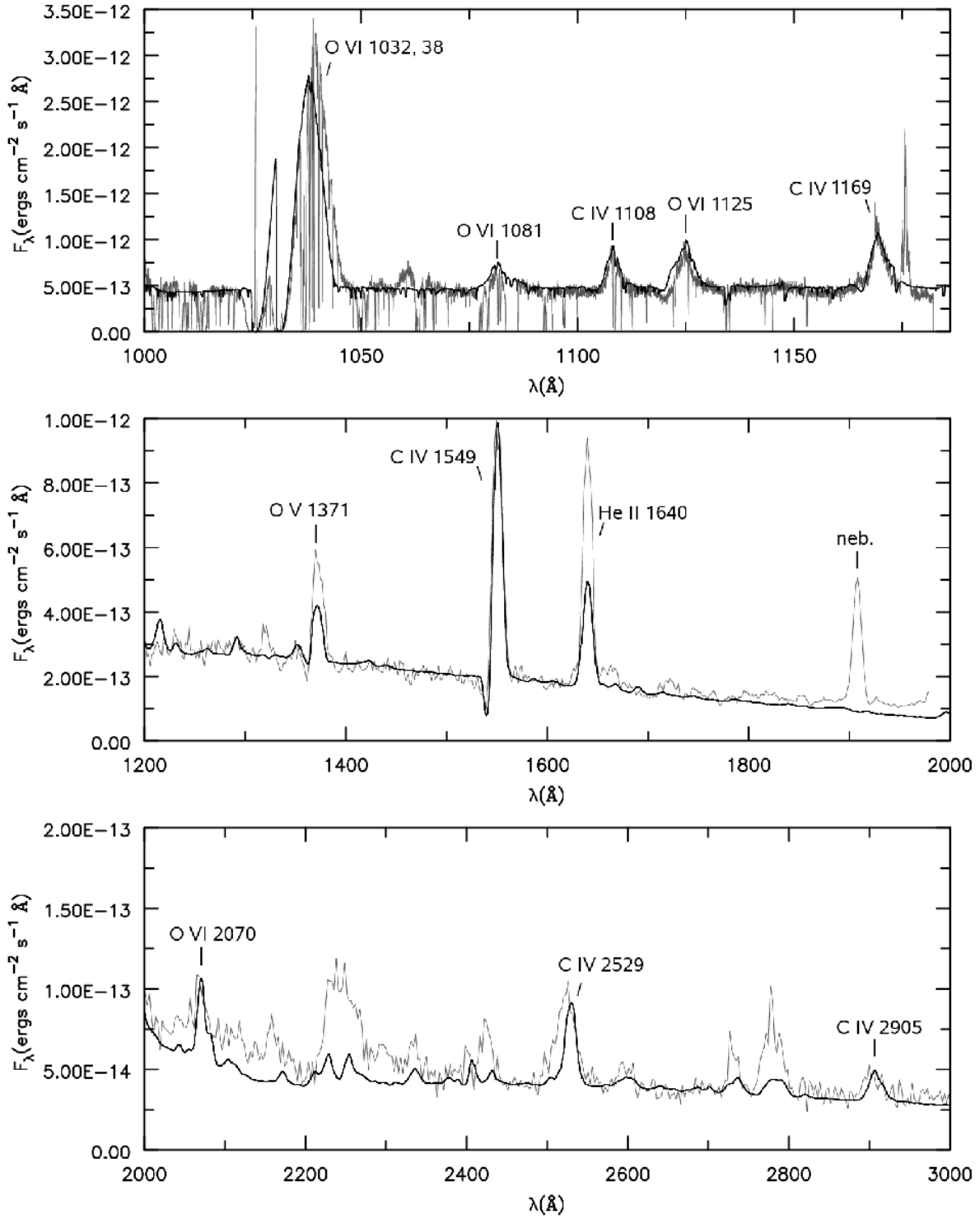


Fig. 11.— NGC 6905 ultraviolet spectra and our model (thick line). Top : FUSE spectrum. Other panels : Low resolution IUE spectra.

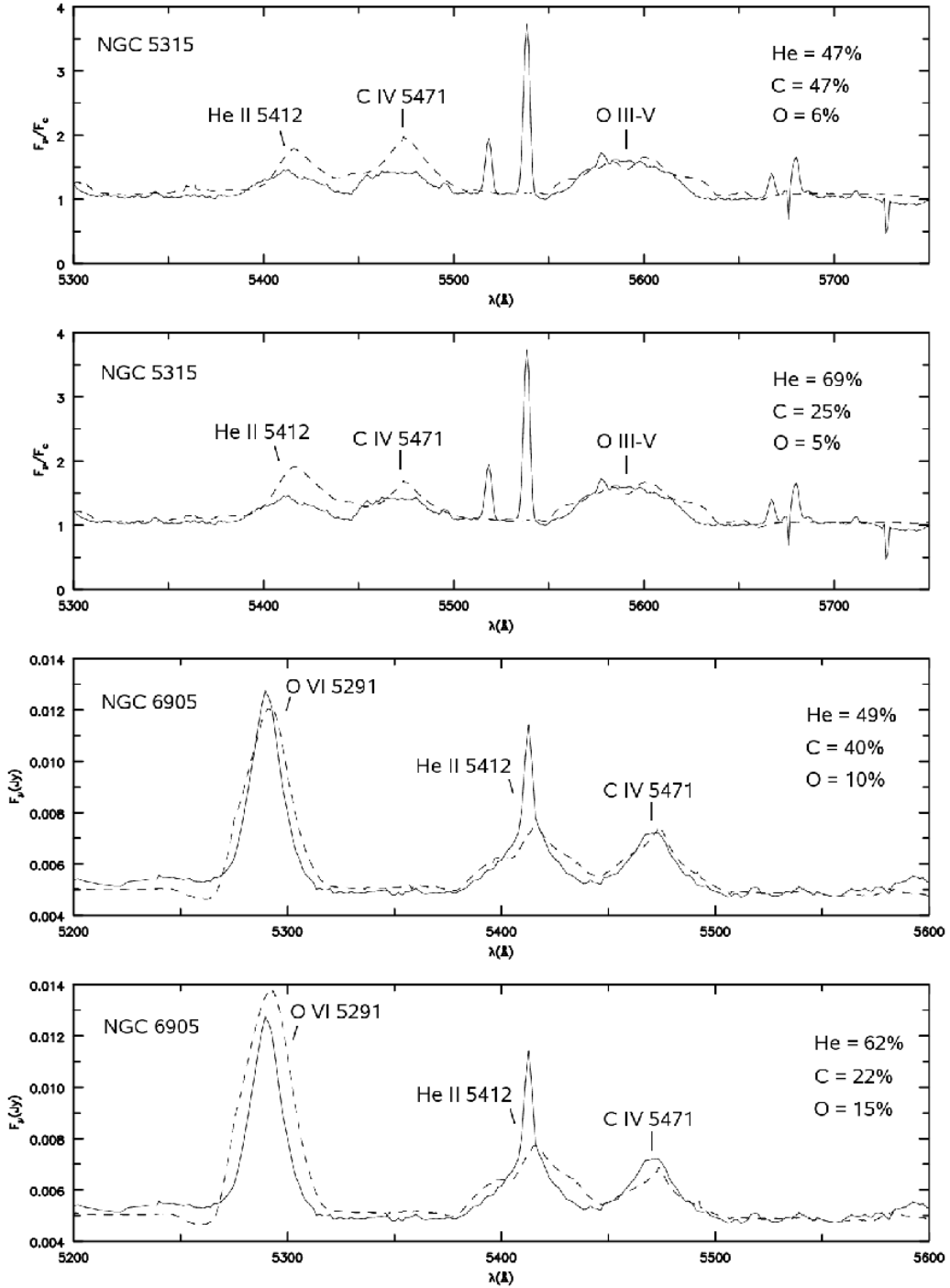


Fig. 12.— Illustration of the effect of variations in the β_C/β_{He} ratio (mass fraction) on the theoretical spectrum of NGC 5315 and NGC 6905. Solid lines are the observational data and dashed lines are the models. Top panel (NGC 5315) : $\beta_C = \beta_{He} = 47\%$ and $\beta_O = 6\%$. 2nd panel (NGC 5315) : $\beta_C = 25\%$, $\beta_{He} = 69\%$ and $\beta_O = 5\%$. 3rd panel (NGC 6905) : $\beta_C = 40\%$, $\beta_{He} = 49\%$ and $\beta_O = 10\%$. 4th panel (NGC 6905) : $\beta_C = 22\%$, $\beta_{He} = 62\%$ and $\beta_O = 15\%$.

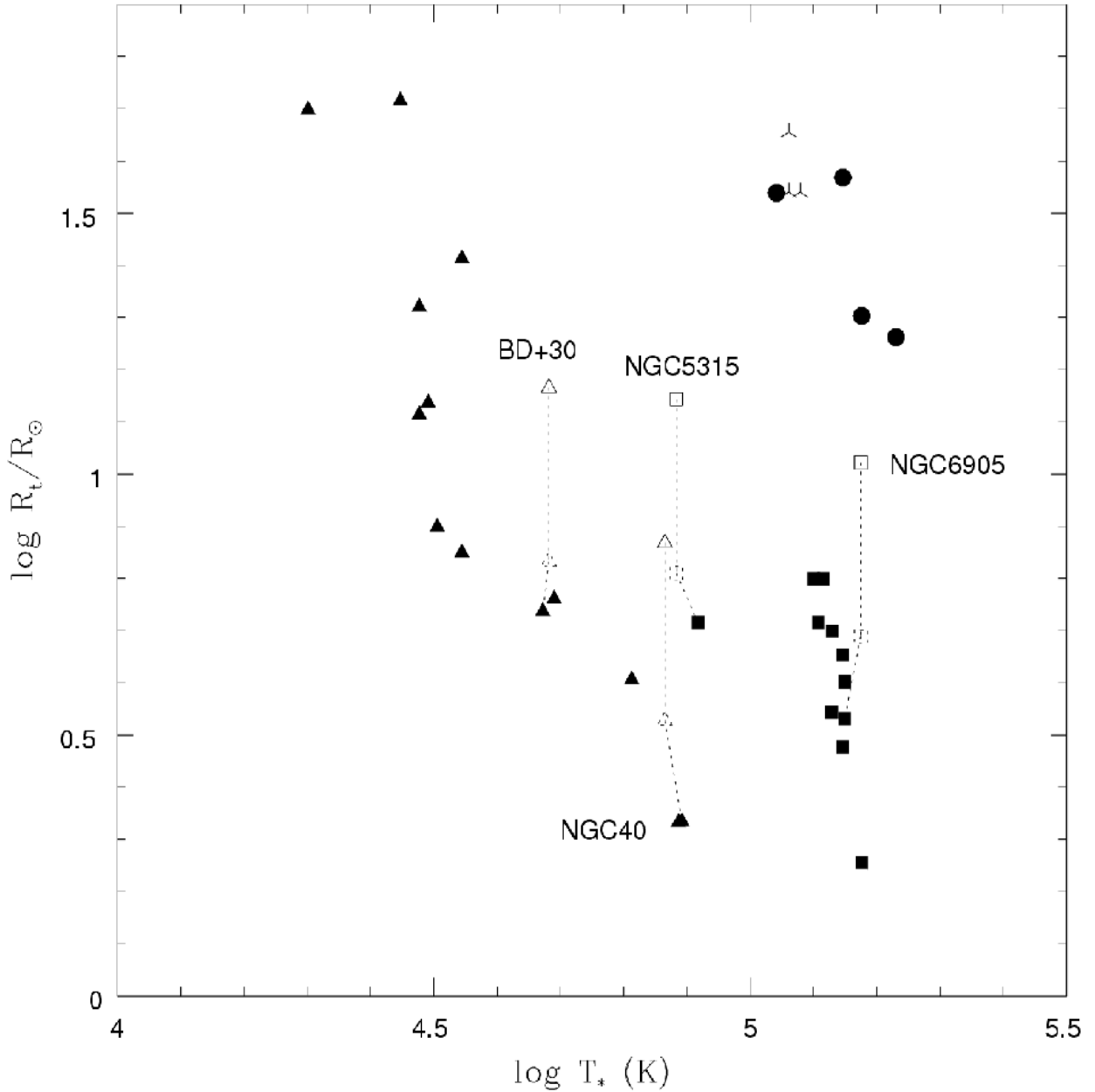


Fig. 13.— Evolutionary sequence in the $\log R_T \times \log T_*$ diagram. Literature data are represented by filled symbols (see Koesterke 2001 and references therein). [WCL] and early-type [WR] stars are represented by triangles and squares, respectively. Crosses indicate [WELS] and PG 1159 stars are represented by circles. Open solid symbols represent our clumped models (with $f = 0.1$) and dashed symbols our un-clumped models. Dashed lines connect them and previous results of the Potsdam group.

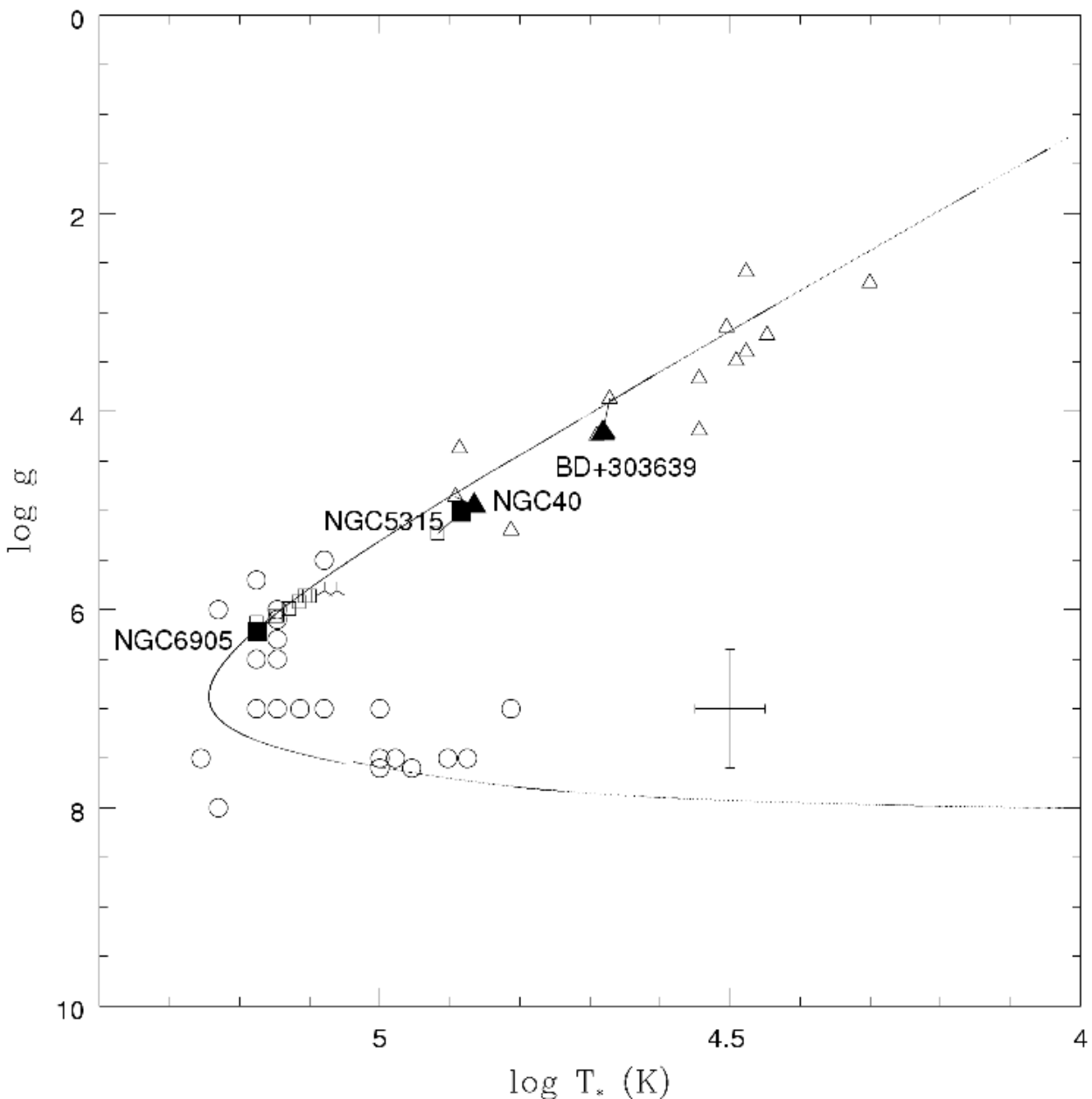


Fig. 14.— Evolutionary sequence in the HR diagram ($\text{Log } g \times \text{Log } T_*$) and values derived by means of non LTE atmosphere models. The track is from Althaus et al. (2005) for a $2.7 M_\odot$ main sequence star that evolved to a $0.5885 M_\odot$ remnant. [WCL] stars are represented by open triangles, early-type [WR] stars by open squares, [WELS] by crosses and PG 1159 by open circles. Our data correspond to filled symbols. Vertical error bars represent an error in distance of a factor of ± 2 , or analogously, a typical spectral uncertainty in the determination of $\text{Log } g$ (see Hügelmeyer et al. 2005). Horizontal error bars illustrate an uncertainty of 10% in temperature determination. Solid lines connect our results with previous works.